Dear Referee #1,

We thank you for the critical comments and suggestions to improve the manuscript (MS). We have considered the comments and modified the MS accordingly. Our detailed responses to the comments are given below.

General comments:

Referee's comment: One of the main problems of the manuscript is that the shown data is not well explained. It is not obvious for the reader understand how the data in each plot has been calculated. Sometimes, this information can be inferred from reading carefully the caption and the references to the figure in the text but this is not always the case and it makes it difficult to read the manuscript. See specific comments. In addition, the manuscript presents a large amount of data in different figures and tables but in some occasions, the discussion of these data is too short.

Authors' response: Major corrections in the revised MS are made. Moreover, answers given to specific comments can be seen in the specific comments section.

Referee's comment: Lack of consistency. The magnitudes and concepts that appear through the text are mentioned in different ways, which makes the reading process very confusing. There are many other inconsistencies, such as the fact that some multi panels are not properly labelled using letters. See specific comments. In addition, there are many formatting issues. Some of them are pointed in the specific comments.

Authors' response: Major corrections in the revised MS are made. Moreover, answers given to specific comments can be seen in the specific comments section.

Referee's comment: The geometry and computational fluid dynamics analysis of 3 passive samplers is given in the section 3. However, there are no references of the BSNE sampler in this section, while in the other sections, the four passive samplers have been mentioned. The geometry and computational fluid analysis of this fourth sampler should be included or at least justify its absence.

Authors' response: Because of resource limitation, we did the CFD analysis only for the three geometries (samplers) and therefore the BSNE was not included in the CFD analysis. Again, answer this specific referees' comment is given in the specific comment section.

Referee's comment: Many comparisons are presented all over the manuscript, but it seems that a significant fraction of the data hasn't been plotted and they appear instead in tables in the SI. I suggest to plot all the data that appears in tables in the SI. Some of the given conclusions regarding to the agreement or disagreement of data need to be revised. See specific comments.

Authors' response: We have now plotted for the whole campaign data showing comparison among samplers. Answers are given in the specific comment section.

Referee's comment: In this manuscript many comparisons in between different instruments are presented. Were the sampling times of each instrument over lapping in all the cases? This remains unexplained, and it seems very unlikely in some occasions, instruments were ran with very different times (24h data compared with 1h data). See specific comments.

Authors' response: The reason why we set up different time interval is because one category of the sampler is operating passively while the other ones (the FWI and the Filter samplers) operate actively. The active ones have a much higher collection velocity. Therefore, we cannot set up the same time interval for both type of samplers, as this would result in either overloading of the active or underloading of one of the passive samplers. A further explanation is given under specific comments.

However, based on the PM_{10} values recorded continuously, we have compared the active sampler interval with the passive samples one and found, that the average PM_{10} values of both intervals differ by 0.2 %. Therefore, we believe that the comparison is justified.

Referee's comment: Regarding to the SEM analysis, were handling blanks taken during the campaign and then analysed under the SEM? In addition, did you test if the particles homogenously distributed over the sampling substrate? If not, this might significantly affect the measurements.

Authors' response: Blank samples were analyzed. The contamination is small for the dust compounds (factor of 30-100 lower than the deposited particle numbers). A low density of pure iron particles is present, apparently already from the manufacturing process. These particles are identified by their chemical composition and removed from the dataset.

Specific comments:

Referee's comment 1: Line 17. "This study focuses on the microphysical properties". This is too vague.

Authors' response: A sentence is added in the revised MS to explain as clearly as possible.

Referee's comment 2: Line 19-32. This paragraph of the abstract looks more like a collection of statements that are made through the paper rather than a paper abstract.

Authors' response: Major corrections in the revised MS are made on abstract part.

Referee's comment 3: Line 20. Acronyms in the abstract have not been defined before.

Authors' response: Correction is made.

Referee's comment 4: Line 26-28. Acronyms defined after they appear for the first time.

Authors' response: Correction is made.

Referee's comment 5: Line 97-98. What about the sampling time of the Flat plate sampler? Were the filters ran for one hour or 24 with the passive samplers?

Authors' response: The sampling time for all passive sampler including the Flat plate sampler was set to be 24 hours. The filters ran for one hour.

Referee's comment 6: Line 149. This section needs a bit more of detail.

Authors' response: More detail on the samples construction and principle is added.

Referee's comment 7: Line 159. The acronym SMPS hasn't been defined. In addition, there are no other references to the SMPS in the main text. Was the data used for this work?

Authors' response: We used data only from OPC. So, corrections in the revised MS are made.

Referee's comment 8: Line 164. How were the samples transported and stored?

Authors' response: All samples were stored in standard SEM storage boxes (Ted Pella Inc, Redding, CA, USA) in dry conditions at room temperature.

Referee's comment 9: Line 170. "Randomly selected areas". Were they randomly generated or were they selected manually by the user?

Authors' response: First, the user orients the microscope the circular deposition area and then the microscope selects smaller sub-areas randomly. So, corrections in the revised MS are made.

Referee's comment 10: Line 194 and 222. Was the temperature dependence considered in the density and dynamic viscosity choice?

Authors' response: We have used constant values for density and dynamic viscosity. It is already mentioned in the MS.

Referee's comment 11: Line 258. I think this section needs to be better explained and describe why and how different models were applied to different samplers

Authors' response: A more detailed explanation is added in section 2.93 in the revised MS (line 276-292).

Referee's comment 12: Line 423. Which was the fraction of mineral dust in the samples? Was it dominating all the sizes? Were the non-mineral dust particles excluded from the calculations?

Authors' response: We found that the fraction of mineral dust in all samples were dominating in all size ranges (96 %) and therefore in calculation, we assumed the fraction of non-dust particles to be negligible.

Referee's comment 13: Line 430. In the mentioned tables, the size distribution for each collected sample is given in both mass flux and number flux. Why has it been described as "Minimum, Maximum and Median Mass Flux $(mg/(m^2d))$ measured by..." in the captions of the table S1, S2, S3, S4, S5 and S6?

Authors' response: In the captions of the table S1, S2, S3, S4, S5 and S6, the unit '$(mg/(m^2d))$' was used for mass flux (mass deposition rate) while the unit '$1/(m^2d)$' was used for number flux (number deposition rate). Corrections are made in the revised electronic supplement.

Referee's comment 14: Line 431. Has all the data in this section been calculated with the SEM? If so indicate. It would be useful to also indicate it in the figure captions.

Authors' response: All mass flux data in the section 4.1.1 is calculated with SEM. A sentence is added in the revised MS to make the information more clear. A sentence is added in the caption too.

Referee's comment 15: Line 435. In this section, the terms "deposition flux" and "mass flux" seem to be used to refer to the same magnitude. If this is the case, use only one notation, and mention alternative notations when the magnitude is introduced first.

Authors' response: Changed to mass deposition rate in the revised MS.

Referee's comment 16: Line449.

"we can clearly see that that there is high temporal variation in deposition flux between dust event days and non-dust event days". Fig. 9 doesn't clearly show this. There is a significant difference for the MWAC sampler, but for the other 3 instruments, the difference doesn't seem "high" for the first four bins (up to a factor 2-3?). This is difficult to see since there are not minor ticks in the y-axis. I suggest to add minor ticks and lines as for the x-axis, as well as softening the statement and explaining better the difference in between the deposition flux during a dust event and a non-dust event.

Authors' response: The plot is modified in the revised MS (see Figure 5 in the revised MS). And also, the statement is modified according to the referee's comment.

Referee's comment 17: Line450.

Line 450. "Generally, the temporal variation is much higher than difference between samplers". This statement seems a bit weak for the reasons mentioned previously (Line 449). In addition, all the data in the tables S1, S2, S3 and S4 hasn't been plotted so, it is difficult to see if these argument is valid for all the data. I think this should be improved by adding more graphs (maybe in the SI) or doing some systematic statistical analysis. Improve this.

Authors' response: a box plot showing temporal variation of size distribution is added to the revised Manuscript.

Referee's comment 18: Line 451. As mentioned before, I suggest to add some y-axis minor ticks or plot it again in a way that allows the reader to understand the differences in the mass fluxes. This has been done for most of the other figures of the manuscript. Reducing the range y-axis range to 10-1 to 104 mg/(m2d) (there is no data at all in the 10-4 to 10-1 mg/(m2d) range) could help to better appreciate the differences between the different curves. Also, explain why some large size bins have been removed (is it due to a small number of particles in those bins?).

The graph is corrected in revised MS. Regarding the last data point, there was not data actively removed. Although particles across all size ranges (up to approximately 100 μm) can be deposited on the passive samplers, in our analysis we did generally not find particles larger than 64 μm diameter. When the last data point is missing from the plots, no particle between 32 and 64 μm was detected.

Referee's comment 19: Line 456-485. In this section, the ratios in between magnitudes obtained with four different instruments have been compared. Why has the Sigma-2 instrument been used as the reference instrument? This section doesn't compare the other instruments within themselves at all. Why? I suggest to add some information about how the other instruments compare to each other or justify why this comparison has been omitted.

Authors' response: The sampler Sigma-2 has been widely used for deposition sampling and therefore, in this work it is used as reference. A comparison showing other samplers as reference is added (see electronic supplement).

Referee's comment 20: Line 473. Having a legend in order to identify the different days could help to understand or discuss why the ratios change that much from one day to each other. Why is the ratio in between the Flat plate and the Sigma-2 of the cyan blue day that low when compared with other days?

Authors' response: A legend is already added to different measurement days to identify the different days and can be seen in the revised MS. The flux ratio of Flat plate to Sigma-2 of the cyan blue day (July 29, 2017) is low when compared with other days. The low value of the deposition rate observed with flat plate for this particular day cannot be explained by other observations, so it has to be considered as an artifact. Therefore, we show the data, but we do not take it into account for further discussion.

Referee's comment 21: Line 474-485. It is very difficult to follow what has been plotted in Fig. 12. Is the blue data the mean ratio between each sampler and the Sigma-2 (same ratios as in the previous section but using number instead of mass)? Has the BSNE deposition velocity ratio modelled data been obtained with the Piskunov model as stated in line 259? They-axis is labelled as deposition velocity ratio, however, ratios of dry deposition flux has been plotted as well. Are these ratios equivalent as one would expect from the equation 7? In general, I think that this figure and what has been plotted in it needs to be much better explained than it is now.

Authors' response: Generally, Fig. 12 (now Figure 8 in the revised MS) shows a comparison of velocity ratios of sampler A to Sampler B obtained from flux measurement to the velocity ratio obtained from different classical deposition velocity models. The ratio of flux measured by one sampler to flux measured by another sampler is equal to the velocity ratio of the two sampler. In the Fig. 12. (now Figure 8 in the revised MS), the blue data shows the velocity ratio obtained from flux measurement while the red one shows the velocity ratios obtained from different deposition velocity models. A table showing different deposition velocity models used for different samplers is added in revised MS in section 2.9.3 (see Table 1). The flux ratios plotted in the Fig. 10 (now Figure 7 in the revised MS) is meant to show the relative collection efficiencies of different sampler with respect to reference sampler (Sigma-2). The paragraph has been rewritten to clarify the type of display.

Referee's comment 22: Line 475. "The deposition velocity ratio from models is often higher than the ratios derived from the mass and number". Is this something that happens in general and has been reported in other studies or does it only happen here? In the first case, add some references.

Authors' response: It is true that the deposition velocity ratio from models is higher than the ratios derived from the mass and number flux. We are not aware of any other studies that have been done on the subject.

However, as this is only a relative display, there cannot be any 'truth' (most accurate sampler) derived. The higher ration can mean an underestimation of the Sima-2 deposition velocity, or an overestimation of the others. This is stated now in the manuscript.

Reviewer comment: Line 487. What has exactly been plotted in Fig. S2? It is not obvious from the description. Explain this properly.

The main purpose of section 4.1.2 to investigate the driving force of atmospheric deposition rate. As already stated in section 4.1.2, Fig. S2 (now Figure S 16 in the revised electronic supplement) displays the correlation between deposition number fluxes (measured by flat plate sampler) and atmospheric number concentration by the OPC. An extended caption has been added to the figure.

Referee's comment 23: Line 489-491. The anti-correlation reported by the authors in the number flux-wind speed data cannot be seen in Fig. S2. Remove this or justify based in some quantitative statistical analysis.

Referee's comment 24: Line 496. Again, two different notations for the dust deposition flux have been used. How is this data related to Fig. S2?

Referee's comment 25: Line 499. What has it been shown in the table 2? From the caption, the reader can understand than dust deposition flux (probably SEM measured) has been correlated to the external measurements of OPC particle number and wind speed. However, in the line 499 the authors suggest that the data in table 2 is a comparison in between the OPC measured concentration and the modelled concentration (using the models on the SEM flux data to obtain this concentrations?). This section is very confusing and unclear and it needs to be much better explained.

Referee's comment 26: Line 503. Do you mean from the correlations inTable2? If so indicate it. In the description of the table it says that the flux was correlated with OPC number concentration, but here the authors mention here PM10. Do you mean number concentration below 10 µm?

description is corrected on the table 2 (now table 3 in the revised MS). And also the size range is explicitly stated now at the beginning of section 4.1.2.

Referee's comment 27: Line 513. How have you plotted the wind speed? Did you divide each day in 30-minute interval averages and then calculated the mean and standard deviation from this data (I guess 48 points per day)? Explain it in the figure caption.

Authors' response: A 30-min averaged wind speed data was obtained by dividing each day data in 30-minute interval averages and then the mean and standard deviation was calculated from this data. An explanation was added into the figure caption in the revised MS.

Referee's comment 28: Line 514. What are the blue boxes showing? Is it the 25 and 75 percentiles? Are the black vertical lines showing only one standard deviation?

Authors' response: Yes. On each blue box, the central mark is the median, the edges of the box are the 25th and 75th percentiles. The black vertical lines show one standard deviation. An explanation was added into the figure caption in the revised MS.

Referee's comment 29: Line 516. "Small particle". Is this a common notation in dust deposition studies to refer to the 1-10 µm size range?

Authors' response: "Small particle" notation was used to refer to PM_{10} size range. Accordingly, the title of section 4.1.2.1 is changed to "Size-resolved apparent deposition velocity in the PM_{10} size range" in the revised MS.

Referee's comment 30: Line 520-521. "The effect of wind speed on deposition velocity is negligible". Why?

Authors' response: As already indicated by Table 2, there is not significant correlation between the wind speed and the observed deposition rate. While this could be still a second order effect of an anticorrelation between atmospheric concentration and wind speed, Fig. 14 (now Figure 9 in the revised MS) shows clearly, that there is not wind speed effect for the smaller particles. While this is in contradiction to the models, one has to keep in mind that the (a) the observed wind speeds are comparatively low here, and (b) the considered size range is not the most affected. An effect of the wind speed might be much stronger at higher wind speed and for larger particles. An according statement is added to the manuscript.

Referee's comment 31: Line 522. In the text, the apparent deposition velocity concept has been introduced as the ratio of the number flux to number concentration. I suggest to use deposition velocity in the y-axis label.

Authors' response: the y-axis label is changed to deposition velocity in the revised MS.

Referee's comment 32: Line 528-529. "Mass concentrations calculated from different passive samplers agree generally well with respect to the statistical uncertainties". This agreement is not fully true for the July 28 and August 21 cases shown in Fig S1. Why?

Authors' response: The agreement generally holds true with the respect to the mean value of the campaign (see Fig. S 9 (right panel) in the revised electronic supplement). And yes, it is correct that agreement might not be true in single cases.

Referee's comment 33: Line 532. Isn't the mas flux example given here the same as in Fig. 9a but with a different y-axis scale? If so, choose another example. Another idea would be removing the whole section and discussing the consistency between samples in a previous section.

Authors' response: The authors are aware of the case that mas flux examples given in section 4.1.3.1 (Fig. 15) and the one in section 4.1.1 (Fig. 9a) are the same, but they do have different message. The message of the Fig. 9a (now Figure 5a in the revised MS) is to show the mass flux measured during dust event day differs from the one measured during non-dust event days (Fig. 9b) (now Figure 5b in the revised MS). The other message of Fig 9a (now Figure 5a in the revised MS) is to show the variation in mass flux measured by different passive samplers (for the same measurement day). The purpose of Fig. 15 (now Figure 10 in the revised MS) is to show the consistence in concentration obtained from flux measurement for different samplers and to show that different deposition velocity models selected for the samplers are generally suitable, despite the deviations in single cases. In addition, one more day is added to Fig. 15 (now Figure 10 in the revised MS).

Referee's comment 34: Line 532. Why does the max flux data measured by the MWAC differ so much from the others but when converting it to mass concentration it agrees with them? The deposition velocity has been calculated with the same model for the MWAC, BSNE and Flat plate.

Authors' response: This seems to be a misunderstanding. MWAC is calculated with the different velocity model (shown in Table 1 in the revised MS). Therefore, the model the observed differences

in deposition rate to a similar range concentration comparatively well. Deposition velocity used for different samplers is explicitly indicated in section 2.9.3 (see table 1 in the revised MS).

Referee's comment 35: Line 532. What is "impaction curve & Piskunov" in the legend? The concept of "impaction curve" hasn't been mentioned before.

Authors' response: The impaction curve was briefly introduced in the method section 2.9.3. To clarify, section 2.9.3 has been reworked and Table 1 added.

Referee's comment 36: Line 540. How were the number size distributions calculated from the flux measurements? This should be better explained here or in the caption.

Authors' response: To get the number concentration size distributions, first the number flux ($\#/(m^2 day)$) measured by different samplers is obtained from SEM. Then, the SEM number flux is converted in to number concentration by using different deposition velocity models. An explanation on how number concentration size distribution is calculated is added in the caption in the revised MS.

Referee's comment 37: Line 544. Why have these specific samples (and these specific instruments) were chosen as an example I assume there are lots of potential comparisons (you sampled during many days with four different instruments). How do other samples taken in other days and/or with other instruments compare the OPC measurements? It seems too arbitrary to show only 4 comparisons out of many and extract some generalist conclusions.

Authors' response: More samples (representing dust event days and non-dust days) are added (see revised electronic supplement). These specific samples shown in the figure (in the MS) are exemplary and they represent a particular dust event day. However, more comparison involving this section can be obtained in the electronic supplement (randomly selected from dust event day and non-dust event day from all samplers.

Referee's comment 38: Line 545. This caption needs to be rewritten in a more clear way. Were the SEM obtained mass flux distribution converted into mass size distributions using the different approaches and then transformed into number size distributions using a density value?

Authors' response: An explanation was given in the previous referee's comment (Referee's comment 36: Line 544). Caption was changed accordingly.

Referee's comment 39: Line 550. The Momentum flux approach data looks black not green

Authors' response: 'The Momentum flux approach' data is changed from green to black in the revised MS.

Referee's comment 40: Line 555. "the above figure (Figure 16)" should be referred as Figure 16 or Fig. 16.

Authors' response: "the above figure (Figure 16)" is changed to Figure 11 (Figure 16 is changed to Figure 11 in the revised MS).

Referee's comment 41: Line 555-560. "also show the comparison of the mass concentration size distribution measurement". Fig. 16 doesn't show any mass size distribution. Please correct or explain this.

Authors' response: In "also show the comparison of the mass concentration size distribution measurement" sentence, 'mass concentration' is replaced by, 'number concentration' in the revised MS.

Referee's comment 42: Line 563. In order to calculate the mass concentration measured by each sampler, don't you have to use the SEM obtained mass flux measurement and assume one of the mentioned models? You haven't mentioned yet a direct method to measure mass concentrations from the passive samplers.

Authors' response: This is correct; we have added a clarification to the caption in the revised MS.

Referee's comment 43: Line 563. When were these samples collected? Why only 2 samples were shown?

Authors' response: The purpose of the figure is to show the comparison of concentration measured by different passive samples with that concentration measured by active sampler (FWI) and OPC. Concentration measured by passive samplers through the campaign (see the electronic supplement). We could do an ESEM analysis only for four days' samples from FWI (which is a total of 12 samples) (from July 26, 2017 to July 29, 2017; each day three measurements) due to limited resources. So we compared the available measurements from passive samples with that of FWI for only of those four days. The two-day measurements (samples) shown in the figure are

arbitrary taken examples and are daily average measurements. They were collected on 26th of July and 27th of July. The information was added in the caption. The authors have analyzed a total of 6 samples from FWI on 26th of July and 27th of July. A clarification is added in the caption in the revised MS. The comparison for all 4 days for FWI yields the same behavior. In addition, in the revised electronic supplement, comparison with remaining two analyzed days of FWI samples are shown.

Referee's comment 44: Line 578. In the methods section, the authors indicate that the sampling time for the passive samplers was about 24 hours while for the FWI was only half an hour. Why have you plotted data that has been collected in such a different time interval?

Authors' response: The reason why we set up different time interval is because one category of the sampler is operating passively while the other one, which is, a FWI operates actively. Therefor we cannot set up the same time interval for both types of samplers. FWI as an active sampler needs less time than the passive ones. However, we calculated from OPC the average PM_{10} for the hours of the FWI samplings and compare it with the PM_{10} of the respective deposition samplings from OPC and we found that the average PM_{10} values of both intervals differ by 2 %. Therefore, we think it is justified to compare samples from FWI and other passive samplers collected with different time interval.

Referee's comment 45: Line 563. It is very difficult to see the y-axis scale. Could you add some minor ticks?

Authors' response: The minor ticks are added in the y-axis scale (see the revised MS).

Referee's comment 46: Line 569-571. What could be causing the disagreement at large sizes?

Authors' response: This is more of a speculation, but the FWIs inherently don't have an inlet at all, whereas all of the passive samplers have an inlet like structure, so the large particles might not be able to enter the inlet, when due to the atmospheric wind direction fluctuations the wind vector is not in parallel with the inlet axis. Also other types of inlet losses in the growing boundary layer might occur, which are not regarded by the models. We have added a cautious sentence on that.

Referee's comment 47: Line 578. Have you used a model to calculate the mass concentration from the mass flux measurements and then transformed this to number concentration?

Authors' response: From SEM measurements, both the number and mass deposition rate are obtained for each single particle. So the same size-resolved model can be applied to convert the deposition rates into number size concentrations. We have added an explicit statement to the method section 2.9.

Referee's comment 48: Line 578. Why only BSNE measurements have been shown? Are they representative of the other passive samplers?

Authors' response: In section 4.1.2 (table 2 (now table 3 in the revised MS)), the authors showed that BSNE is actually a suitable instrument for a PM_{10} estimation. In this connection, the authors showed the comparison of number concentration measured with Filter-sampler method, BSNE and OPC. Measurements by other samplers are shown in the electronic supplement.

Referee's comment 49: Line 578. In the methods section, the authors indicate that the sampling time for the passive samplers was about 24 hours while for the filter samples was only one hour. Why have you plotted data that has been collected in such a different time interval?

Authors' response: Please refer to the answer to comment 44.

Referee's comment 50: Line 581. Was the data in this section obtained following the same SEM approach as for the flat plate sampler? These measurements need to be described more precisely.

Authors' response: The same SEM approach has been used in this section also. The only difference is that the flat plate geometry with 25 mm-stub used here to collect particles where as in the flat plate described in the previous section, the stub was 12 mm size was used. Precise description for the upward and downward flux measurement has been indicated in the section 2.4 in the revised MS.

Referee's comment 51: Line 595. When were this samples taken?

Authors' response: A legend is added to show different sampling dates (see the revised MS).

Referee's comment 52: Line 599. As mentioned before, why hasn't the BSNE included in this analysis? Explain.

Authors' response: Due to resource limitations, please refer to the comment above.

Referee's comment 53: Line 609. It is difficult to see agreement in between the Stokes model and the CFD for the MWAC sampler in Fig. 20.

Authors' response: Indeed, the agreement is poor in general. Regarding the mentioned models and sampler, this appears to be a misunderstanding regarding the 'general agreement'. it has been rephrased in the revised MS.

Referee's comment 54: Line 623. Why haven't the errors been propagated?

Authors' response: Refer to the revised MS for explanation.

Referee's comment 55: Line 626. What do the vertical clusters of data mean? Why are there so many measurements aligned? (Particularly in the d, e and f case).

Authors' response: The vertical clusters of data mean that for different wind speed situations, similar ratios are measured, where the models would predict different ratios. This was already seen above, where in contrast to the model prediction, no wind speed dependence was observed.

Referee's comment 56: Line 627. Has all the collected data been presented here

Authors' response: All collected data (i.e. simultaneously analyzed samples from different samplers) has been analyzed and is show here.

Referee's comment 57: Line 645-646. "atmospheric concentrations can be calculated from different sampler deposition fluxes, which are more in agreement". The statement about the increase in the agreement is a bit vague. In addition, it seems that only a subset of all the possible atmospheric concentration samples has been shown

Authors' response: More data (campaign average) is added and the plot can be seen in the revised electronic supplement. The samplers are better in agreement with respect to the average, when the models are employed to calculate the concentration, but temporal variation correlation does not get better.

Referee's comment 58: Line 648-649. "In particular when considering the size-resolved deposition velocities and flux ratios, great discrepancies show up". More detail in which deposition velocities and flux ratios is needed here.

Authors' response: See the revised MS for explanation.

Referee's comment 59: Line 652-656. This paragraph describes again about the size-resolved concentration. Reduce it and merge it with the first paragraph that describes this (643-647).

Authors' response: The paragraph is reduced and merged into line 643-647 (see the revised MS).

Referee's comment 60: Line 664-667. It seems that not all the data has been shown, therefore the reader cannot check this conclusion

Authors' response: More data is shown now in the revised MS.

Technical corrections

Referee's comment 61: Line 205. "Ati".There is an "i" after the t in the denominator of the equation. The is missing a p if it is referring to particle density.

Authors' response: Correction is made.

Referee's comment 62: Line 207. Spaces must be included between number and unit (e.g. 2-4 µm).

Authors' response: Correction is made in the revised MS.

Referee's comment 63: Line 227. Does u-s mean us? I suggest use the same notation.

Authors' response: Correction is made in the revised MS.

Referee's comment 64: Line 234. Units appear in the exponential notation in some occasions but in some others they don't. I suggest to use the exponential notation through the whole manuscript (m/s should be written as m s-1)

Authors' response: Majority of the exponential notation Units through the whole manuscript is written in the form of 'a/b' and therefore we changed the units from exponential notation to the 'a/b' form though out the manuscript in the revised MS.

Referee's comment 65: Line 236. "Wood1981". Wood 1981.

Authors' response: Correction is made in the revised MS.

Referee's comment 66: Line 351. Missing coma or full stop

Authors' response: Correction is made in the revised MS.

Referee's comment 67: Line 514. Two notations have been used to describe the observatory. Through most of the text, "Izaña Global Atmospheric Watch observatory" has been used, but

here, a different one has been used. You can mention both at the beginning and then use only one trough the text.

Authors' response: Correction is made in the revised MS.

Referee's comment 68: Line 581. "upward/downward-facing measurements"

Authors' response: We do not understand this comment. The collection surface in this measurement is facing to each other in upward-downward direction and thus the name "upward/downward-facing measurements" is used.

Referee's comment 69: Line 584. "Up-ward" and "Down-ward". Is this the right notation or is it upward and downward?

Authors' response: "Up-ward" and "Down-ward" is replaced by "upward and downward'' in the revised MS.

Referee's comment 70: Line 603. "V-dp" was referred earlier in the paper as Vd. Use a consistent notation

Authors' response: "V-dp" is replaced by "Vd" in the revised MS.

Referee's comment 71: Line 642. "variability of dust".

Authors' response: We do not understand this comment.

General

Referee's comment 72: Missing a, b, c... labelling in the multi panels. Sub-indexes haven't been written in many figures (E.g. u-s instead of us).

Authors' response: multi panels has been labelled with a, b, c… and indicated in the caption. Sub-indexes have been corrected now (see the revised MS).

Dear Mingjin,

We thank you for the critical comments and suggestions to improve the manuscript (MS). We have considered the comments and modified the MS accordingly. Our detailed responses to the comments are given below.

General comments:

For your general comments, major corrections in the revised MS are made. Moreover, answers given to specific comments can be seen in the specific comments section.

Specific comments:

Comment:

I feel there are too many figures used in the manuscript. For example, Fig. 4-7 present

CFD results, and do they have to be included in the manuscript? Can some of them be moved

into the supplement? There are only three points in Fig. 8, and so is it necessary to have this

figure?

Authors' response: Some of the figures present in the CFD result (Fig. 4-7) are now moved to electronic supplement (see the revised electronic supplement). In Fig. 8, we wanted to show how the mean flow velocity in the MWAC tube varies as a function of the outside velocity for the three cases. We have also moved Fig. 8 to the electronic supplement.

Comment: Line 457-460. Figure 13 is mentioned before Figure 10, and it took me a while to find Figure 13. In addition, can Fig. 13 be moved to supplement?

Authors' response: The figure is now moved to the supplement.

Comment: Line 553-554, line 651, line 641-642, and etc.: Quite frequently there are paragraphs which contain 1-2 short sentences. This makes the manuscript very fragmented and hard to follow.

Authors' response: Correction is made in the revised MS.

Comment: Line 38: The paper by Jickells et al. (2005) in fact discusses the effect of mineral dust on oceanic biogeochemistry and thus should not be cited here. Instead, it should be cited in line 40-

41. In addition, please consider citing new references instead of papers which were published >20 years ago.

Authors' response: Correction is made in the revised MS. Quite a few references we used are old indeed; but we cannot leave them as of our formulations are based on them.

Referee's comment: Line 13: change "As result" to "As a result"; Line 42: change "is ranging" to "ranging"; Line 56: change "on addition" to "in addition"; line 84: change "station shields" to "station, shields". There are many grammatical errors and awkward sentences in the manuscript, and careful editing of the manuscript is needed.

Authors' response: Correction is made in the revised MS.

Field comparison of dry deposition samplers for collection of atmospheric mineral dust: results from single-particle characterization

Andebo Waza[1], Kilian Schneiders[1], Jan May[2], Sergio Rodríguez[3, 4], Bernd Epple[2], Konrad Kandler[1]

1Atmospheric Aerosol, Institute for Applied Geosciences, Technische Universität Darmstadt, D-64287 Darmstadt, Germany

2Institute for Energy Systems & Technology, Technische Universität Darmstadt, D-64287 Darmstadt, Germany

3Izaña Atmospheric Research Centre, AEMET, Tenerife, Spain.

4Estación Experimental de Zonas Aridas, EEZA CSIC, Almería, Spain.

*correspondence to andebo.waza@geo.tu-darmstadt.de

Abstract

Frequently, passive dry deposition collectors are used to sample atmospheric dust deposition. However, there exists a multitude of different instruments with different, usually not well-characterized sampling efficiencies. As a result, the acquired data might be considerably biased with respect to their size representativity, and as consequence, also composition. In this study, individual particle analysis by automated scanning electron microscopy coupled with energy-dispersive X-ray was used to characterize different, commonly used passive samplers with respect to their size-resolved deposition rate and concentration. This study focuses on the microphysical properties, i.e. the aerosol concentration and deposition rates as well as the particle size distributions. In addition, computational fluid dynamics modeling was used in parallel to achieve deposition velocities from a theoretical point of view.

SEM calculated deposition rate measurements made using different passive samplers show a disagreement among the samplers. Modified Wilson and Cooke (MWAC) and Big Spring Number Eight (BSNE) - both horizontal flux samplers - collect considerably more material than Flat plate and the Sigma-2, which are vertical flux samplers. The collection efficiency of MWAC increases for large particles in comparison to Sigma-2 with increasing wind speed, while such an increase is less observed in the case of BSNE. A positive correlation is found between deposition rate and PM_{10} concentration measurements by an optical particle spectrometer. The results indicate that a BSNE and Sigma-2 can be good options for PM_{10} measurement, whereas MWAC and Flat plate samplers are not a suitable choice. A negative correlation was observed in between dust deposition rate and wind speed. Deposition velocities calculated from different classical deposition models do not agree with deposition velocities estimated using computational fluid dynamics simulations (CFD). The deposition velocity estimated

from CFD was often higher than the values derived from classical deposition velocity models. Moreover, the modeled deposition velocitiy ratios between different samplers do not agree with the observations.

Key words: Mineral dust particles, passive samplers, SEM-EDX, single particle analysis, computational fluid dynamics

1 Introduction

Mineral dust aerosol in the climate system has received considerable scientific attention mainly due to its direct effect on the radiative budget and indirect one on cloud microphysical properties (Arimoto, 2001; Huang et al., 2010). Mineral dust particles also play a key part with respect to gas phase chemistry by providing a reaction surface e.g. ozone depletion (Nicolas et al., 2009; Prospero et al., 1995). Moreover, dust aerosol also plays an important role in biogeochemical cycles by supplying important and limiting nutrients to Ocean surfaces (Jickells et al., 2005). Mineral dust is emitted mainly from the arid and semi-arid regions of the world and believed to have a global source strength ranging from 1000-3000 Tgyr^{-1} (Andreae, 1995). They form the single largest component of global atmospheric aerosol mass budget, contributing about one third of the total natural aerosol mass annually (Penner et al., 2001).

Deposition measurement data of mineral dust are useful to validate numerical simulation models and to improve our understanding of deposition processes. However, the scarcity and the limited representatively of the deposition measurement data for validation pose a major challenge to assess dust deposition at regional and global scales (Schulz et al., 2012; WMO, 2011). This is in part linked to the uncertainties evolving from the use of different and non-standardized measurement techniques.

Commonly, deposition is measured by passive techniques, which provide an acceptor area for the depositing atmospheric particles. The advantage of these passive samplers is that they operate passively, resulting in simple and thus cheaper instruments, so that many locations can be sampled at a reasonable cost (Goossens and Buck, 2012). The usual lack of a power supply allows also for unattended remote setups. However, the most important disadvantage is that collection efficiency and deposition velocity is determined by the environmental conditions not under operator control, and in remote setups also frequently also unknown. That implies, in addition, that the sampler shape can have a strong and variable impact of the collection properties.

While there is previous work describing and modeling single samplers (Einstein et al., 2012; Wagner and Leith, 2001a, b; Yamamoto et al., 2006) and a few comparison studies (Goossens and Buck, 2012; Mendez et al., 2016), most previous studies (Goossens and Buck, 2012; López-García et al., 2013) only

compare total mass, thereby neglecting size dependence and potential comparison biases. Also, a systematic assessment of the impact of wind conditions is not commonly carried out, but for example Mendez et al. (2016) showed that the efficiency of the BSNE and MWAC samplers for collecting PM_{10} varies with wind speed, and Goossens and Buck (2012) found that PM_{10} concentrations from BSNE and DustTrak samplers have comparable values for wind speeds from 2–7 m/s.

The purpose of this study is to assess the particle collection properties of different deposition and other passive samplers based on single particle measurements, and to assess their agreement with theory. From the available data, also relations of the collected particle microphysics and composition homogeneity between the samplers will be presented, which can be used as estimators for the comparability of previous literature data based on the different techniques. To the best of our knowledge, this is the first study to analyze dry deposition measurements collected using passive samplers by means of a single-particle SEM-EDX Analysis approach (particularly in the size fraction larger than 10 μm).

2 Material and methods

2.1 Sampling location and time

Sahara and Sahel provide large quantities of soil dust, resulting in a westward flow of mineral dust particles over the North Atlantic Ocean accounting for up to 50% of global dust budget (Goudie and Middleton, 2001). Owing to proximity to the African continent, the Canary Islands are influenced by dust particles transported from Sahara and Sahel regions. Therefore, Tenerife is one of the best locations to study relevant dust aerosol in a natural environment.

For this study, we conducted a two month (July to August 2017) aerosol collection and dry deposition sampling campaign at Izaña Global Atmospheric Watch observatory (Bergamaschi et al., 2000; Rodríguez et al., 2015) (28.3085ºN, 16.4995ºW). Sampling inlet were placed at a height of 2 m above ground, on top of a measurement installation. The installation was made on a 160 m^2 flat concrete platform. The trade wind inversion, which is a typical meteorological feature of the station, shields most of the time the observatory from local island emissions (García et al., 2016). Therefore, the Izaña Global Atmospheric Watch observatory is an ideal choice for in-situ measurements under "free troposphere" conditions (Bergamaschi et al., 2000; García et al., 2016).

2.2 Wind measurements

An ultra-sonic anemometer (Young model 81000, R. M. Young Company, Traverse City, MI, USA) was installed at approximately 2 m height above the ground to obtain the 3-D wind velocity and direction. It was operated with a time resolution of 10 Hz to get basic information on turbulence structure.

2.3 Particle sampling

Samples were collected from different, commonly used samplers, namely Big Spring Number Eight (BSNE) (Fryrear, 1986), Modified Wilson and Cooke (MWAC) (Wilson and Cook, 1980), Sigma-2 (VDI2119, 2013) and Flat plate (UNC-derived) (Ott and Peters, 2008). In addition, the free-wing impactor (FWI) (Kandler et al., 2018) was used to collect coarser particles. The BSNE, MWAC, FWI and Filter Sampler were mounted on wind vanes to align them to the ambient wind direction. Samples were collected continuously, and substrates were exchanged at intervals of 24 hours. The sampling duration for FWI (12 mm Al-stub) was 30 min only to avoid overloading. The sampling duration for filter sampler was set to be one hour. It has to be noted that the PM_{10} from optical measurements for this particular 0.5 or 1 hour only deviates by 2 % and 0.2 % respectively from the 24-h-average.

2.3.1 Flat plate sampler

The Flat plate sampler used in this work was taken from the original Flat plate geometry used in Ott and Peters (2008). Briefly, the geometry contains two round brass plates (top plate diameter 203 mm, bottom plate 127 mm, thickness 1 mm each) mounted in a distance of 16 mm. Unlike the original design, the geometry of the current work has a cylindrical dip in the lower plate, which recedes the sampling substrate – a SEM stub with a thickness of 3.2 mm – from the airflow, thereby reducing the flow disturbance. A preliminary study with the modified and original setup side-by-side in a rural environment had shown that this recession approximately doubles the collection efficiency for large particles. In this design, larger droplets (> 1 mm) are prevented by this setup from reaching the SEM stub surface at the local wind speeds Ott and Peters (2008). As described in Wagner and Leith (2001a); (Wagner and Leith, 2001b), the main triggers for particle deposition on the substrates for this sampler are diffusion, gravity settling, and turbulent inertial forces, of which only the latter two are relevant in our study.

2.3.2 Sigma-2 sampler

The Sigma-2 sampling device is described in Dietze et al. (2006); (Schultz, 1989; VDI2119, 2013). Briefly, the geometry consists of a cylindrical sedimentation tube with a height of about 27 cm made of antistatic plastic, which is topped by a protective cap with diameter of 158 mm. At its top, the cap has

118   four rectangular inlet windows (measuring 40 mm x 77 mm, all at the same height) at its side providing

119   away for passive entrance of particles to the collection surface. Once entered the tube, particles are

120   assumed settle down to the collection surface due to gravitation (Stokes' law) (VDI2119, 2013). The

121   samplers designed in a way that it protects the sample from direct radiation, wind and precipitation.

122   2.3.3   The Modified Wilson and Cooke (MWAC) sampler

123   The MWAC sampler is based on an original design developed by Wilson and Cook (1980). The sampler

124   consists of a closed polyethylene bottle, serving as settling chamber, to which an inlet tube and an outlet

125   tube have been added. The MWAC sampling bottles are 95 mm long with a diameter of 48 mm. The two

126   inlet and outlet plastic tubes with inner and outer diameter 8 and 10 mm respectively, pass air through

127   the cap into the bottle and then out again. The large volume of the bottle relative to the inlet diameter

128   makes the dust particles entering the bottle to be deposited in the bottle due to the flow deceleration the

129   total bottle area, and due to impaction below the exit of the inlet tube. The air then discharges from the

130   bottle via the outlet tube. MWAC is one of the most commonly used samplers (Goossens and Offer,

131   2000) and has a high sampling efficiency for large particles (Mendez et al., 2016).

132   2.3.4   The Big Spring Number Eight (BSNE) sampler

133   The BSNE sampler, originally designed by Fryrear (1986), is intended to collect airborne dust particles

134   from the horizontal flux (Goossens and Offer, 2000). Briefly, the particle laden air passes through a

135   rectangular inlet (21 mm wide and 11 mm high, with total area of 231 mm^2). Once inside the sampler,

136   air speed is reduced by continuous cross section increase (angular walls) and the particles settle out on a

137   collection surface. Air discharges through a mesh screen.

138   2.3.5   Free-wing impactor (FWI)

139   A free rotating wing impactor (Jaenicke and Junge, 1967; Kandler et al., 2018; Kandler et al., 2009) was

140   used to collect particles larger than approximately 5 μm. A FWI has a sticky impaction surface attached

141   to a rotating arm that moves through air; particles deposit on the moving plate due to their inertia. The

142   rotating arm is moved at constant speed by a stepper motor, which is fixed on a wind vane, aligning the

143   FWI to wind direction. The particle size cut-off is defined by the impaction parameter, i.e. by rotation

144   speed, wind speed and sample substrate geometry. Details of working principle of FWI can be obtained

145   from Kandler et al. (2018)

2.3.6 Filter sampler

A filter sampler with Nucleopore filters (Whatman® Nuclepore™ Track-Etched Membranes diam. 25 mm, pore size 0.4 μm, polycarbonate) mounted on a wind vane was used for iso-axial particle collection. An inlet nozzle of 6 mm was used to achieve pseudo-isokinetic conditions. Sample flow (0.75 m³/h volumetric at ambient conditions) was measured by a mass flow meter (MASS-STREAM, M+W instruments, Leonhardsbuch, Germany). The filter sampler was operated at least two times a day.

2.4 Upward-downward deposition rate sampler

It is important to compare the upward and downward rates to understand the turbulent and the gravitational share in aerosol deposition rate measurement. Following an approach by Noll and Fang (1989), it was assumed that turbulent transport is the main mechanism for upward-directed deposition rate while turbulent transport and sedimentation are the mechanism of for the downward one. Therefore, a sampler with an upward- and a downward-facing substrate in analogy to the Flat plate sampler was designed. Air is flowing between two circular steel plates thick 1 mm with a diameter of 127 mm. In the centers of the plates, two substrates are mounted opposite to each other. The substrate holders are recessed, so that their adhesive collection surface is in plane with the steel surface. The construction is mounted into a frame with a distance of 16 mm between the plates / substrates.

2.5 Ancillary Aerosol Data

Additional information regarding the aerosol particle size distributions has been obtained by using an optical particle counter (OPC, GRIMM, Ainring, Germany), which is operationally available at the Izaña Global Atmospheric Watch observatory (Bergamaschi et al., 2000; Rodríguez et al., 2015).

2.6 SEM-Analysis

All aerosol samples (except the filter sampler) were collected on pure carbon adhesive substrates (Spectro Tabs, Plano GmbH, Wetzlar, Germany) mounted to standard SEM aluminum stubs. The filter samples were stored in standard 'Petrislides' (Merck KGaA, Darmstadt, Germany). All adhesive samples were stored in standard SEM storage boxes (Ted Pella Inc, Redding, CA, USA) in dry conditions at room temperature. Individual particle analysis by automated scanning electron microscopy (SEM; FEI ESEM Quanta 400 FEG, FEI, Eindhoven, The Netherlands; operated at 12.5 kV, lateral beam extension 3 nm approx., spatial resolution 160 nm) was used to characterize particles for size and composition. A total of 316,000 particles from six samplers was analyzed. 26 samples from BSNE (53,000 particles), 23 samples from MWAC (49,000), 23 samples from SIGMA-2 (39,000), 18 samples from Flat plate (12 mm) (24,000), 22 samples from Flat plate (25 mm) (21,000), 13 samples from Filter (80,000) and 12

177   samples from FWI-12 mm (50,000) were analyzed. Each sample was characterized at areas selected by

178   a random generator, until a total of 3,000 particles with projected area diameters greater than 1 μm was

179   reached. For particle identification, the backscattered electron image (BSE-image) has been used, as dust

180   particles contain elements with higher atomic number than carbon and therefore appear as detectable

181   bright spots in the BSE-image.

182   Chemistry information was derived by energy-dispersive X-ray analysis (EDX; Oxford X-Max 120,

183   Oxford Instruments, Abingdon, United Kingdom). The internal ZAF-correction of the detector / software

184   system – based on inter-peak background radiation absorption measurements for correction – was used

185   for obtaining quantitative results.

186   **2.7   Particle size determination**

187   The image analysis integrated into the SEM-EDX software determines the size of particles as a projected

188   area diameter.

189     $$\mathbf{d_g} = \sqrt{\frac{4B}{\pi}} \qquad\qquad (1)$$

190   Where $\mathbf{B}$ and $\boldsymbol{d_g}$ are the area covered by the particle on the sample substrate and the projected area

191   diameter respectively.

192   Following Ott et al. (2008), the volumetric shape factor, $\boldsymbol{S_v}$ is determined from the count data as:

193     $$S_v = \frac{P^2}{4\pi A} \qquad\qquad (2)$$

194   Where P and A are the perimeter and the projected area of the particle respectively.

195   The volume-equivalent diameter (sphere with the same volume as the irregular shaped particle) is then,

196   calculated from the projected area diameter via the volumetric shape factor (Ott et al., 2008) and is

197   expressed by particle projected area and perimeter as

198     $$d_v = \frac{4\pi B}{P^2} dg = \frac{1}{P^2}\sqrt{64\pi B^3} \qquad\qquad (3)$$

199   The aerodynamic diameter (d_a) is calculated from projected area diameter through the use of a volumetric

200   shape factor and aerodynamic shape factor (Wagner and Leith, 2001b)

201     $$d_a = \sqrt{[d_v\,(\rho_p/\rho_0)1/S_d)]} \qquad\qquad (4)$$

With S_d the aerodynamic shape factor; ρ_p and ρ_0 are particle density and unit density respectively. For this work, a value of $S_d = 1.41$ was used (Davies, 1979). Cunningham's slip correction was neglected in this study, as all particles considered were super-micron size.

2.8 Mass and number deposition rate calculation

The mass deposition rate (MDR) and number deposition rate (NDR) are calculated from deposited particle numbers per area, individual particle size and, in case of MDR, density. The particle density was assumed to be equal the bulk material density of the dominating identified compound for each particle (Kandler et al., 2007). A window correction (Kandler et al., 2009) was applied to the particle deposition rate as:

$$C_w = \frac{w_x w_y}{(w_x - d_p)(w_y - d_p)} \tag{5}$$

Where w_x and w_y are the dimensions of the analysis rectangle.

The MDR of the samples is then determined as

$$MDR = \frac{1}{Ati} \sum_k \rho \, d_p^3 C_w(d_p, k) \tag{6}$$

Similarly, The NDR of the samples is determined as

$$NDR = \frac{1}{Ati} \sum_k C_w(d_p, k) \tag{7}$$

With A is the total analyzed area, t is the sample collection time, ρ particle density and k is index of the particle.

Size distributions for all properties were calculated for the logarithmic-equidistant intervals of 1-2 μm, 2-4 μm, 4-8 μm, 8-16 μm, 16-32 μm, and 32-64 μm.

2.9 Modeling atmospheric concentrations and size distributions from flux measurements

Concentrations are calculated from the deposition rate using different deposition velocity models for different samples, namely the models of Stokes and Piskunov (Piskunov, 2009). The basic relationship between concentration and deposition rate was already given by Junge (1963), as the ratio of deposition rate to concentration:

$$V_d = F/C \tag{8}$$

With F is deposition rate and C is concentration. Note that the formulation is independent of the type of concentration, i.e. it can be equally applied to number or mass concentrations.

229 All different approaches now give different formulations for the deposition velocity, based on a set of
230 assumptions and neglections.

231 2.9.1 Stokes settling

232 Terminal settling velocity (V_{ts}) is calculated according to Stokes' law.

233 $$V_{ts} = \frac{d_p^2 g(\rho_p - \rho_a)}{18\mu} \tag{9}$$

234 Where d_p is the particle size, g is the gravitational acceleration (9.81 m/s^2); ρ_p the density of particle; ρ_a
235 the air density; μ is the dynamic viscosity of air (1.8*10^{-5} kg/(ms)).

236 2.9.2 Turbulent deposition and more complex deposition models

237 To calculate the turbulent impaction velocity, which depends of the wind speed, the friction velocity is
238 needed. Friction velocity (u_*), which is a measure of wind generated turbulence is one most important
239 variables affecting deposition velocity (Arya, 1977). Mainly two different approaches have been used to
240 estimate u_*. On one hand the momentum flux or the eddy covariance (EC) approach (Ettling, 1996),
241 which directly estimates u_* from the correlations between the measured horizontal and vertical wind
242 velocity fluctuation, and on the other the law of the wall (LoW) approach (Shao et al., 2011), which
243 estimates u_* from the wind profile. The latter can be approximated from free-stream velocity and
244 roughness assumptions (Wood, 1981), where the flow inside the sampler is assumed to be in the
245 hydraulically smooth regime (Schlichting, 1968). **Figure 1** shows correlations between u_* estimated
246 using Wood (1981) and Ettling (1996) approaches. Obviously, the approaches lead to different results,
247 for which no clear explanation is available (Dupont et al., 2018) .
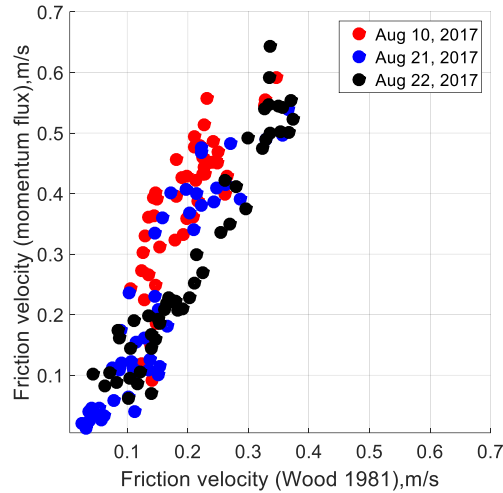
Figure 1: Comparison of the friction velocities obtained from the momentum flux and the Wood 1981 approaches for different days with different wind speeds (average wind speed =2.9 m/s, 2.1 m/s, 3.1 m/s for Aug 10, Aug 21, and Aug 22, 2017, respectively).

For the current work, the friction velocity is calculation is based on Wood (1981) approach:

$$u_* = (u/\sqrt{2}) \, [(2log10(Re) - 0.65)^{-1.15}] \tag{10}$$

Where Re is the flow Reynolds number at the sampling stub location and is given as

$$Re = uX/V \tag{11}$$

X is the distance from the lower plate edge to the center of the sampling stub (6.3 cm) and V is kinematic viscosity.

The reason why we opted to use the Wood (1981) over the Ettling (1996) approach is a) its simplicity, as it requires only average wind speeds instead of 3D high resolution ones, and therefore will be more commonly applicable; and b) the fact that the momentum approach yields sometimes uninterpretable data, in particular in case of buoyancy-driven flow. For some case studies, both approaches are compared below.

There are a variety of models estimating the particles deposition speed (Aluko and Noll, 2006; Noll and Fang, 1989; Noll et al., 2001; Piskunov, 2009; Slinn and Slinn, 1980; Wagner and Leith, 2001a) (see **Figure 2**). And these different deposition velocity models yield different results, which could be due to negligence of unaccounted forces (Lai and Nazaroff, 2005) or due to the way how friction velocity is

267 determined or can be related to suppositions by different models (Kandler et al., 2018). Unless otherwise
268 stated, the particle density used in deposition velocity calculation is 2600 kg/m^3.

269 It can be noted that a particular deposition model therefore may not be suitable in different cases for
270 describing the deposition velocity precisely, so as a result concentrations derived from deposition rate
271 measurements are likely to be biased (Giardina and Buffa, 2018; Kandler et al., 2018).

272
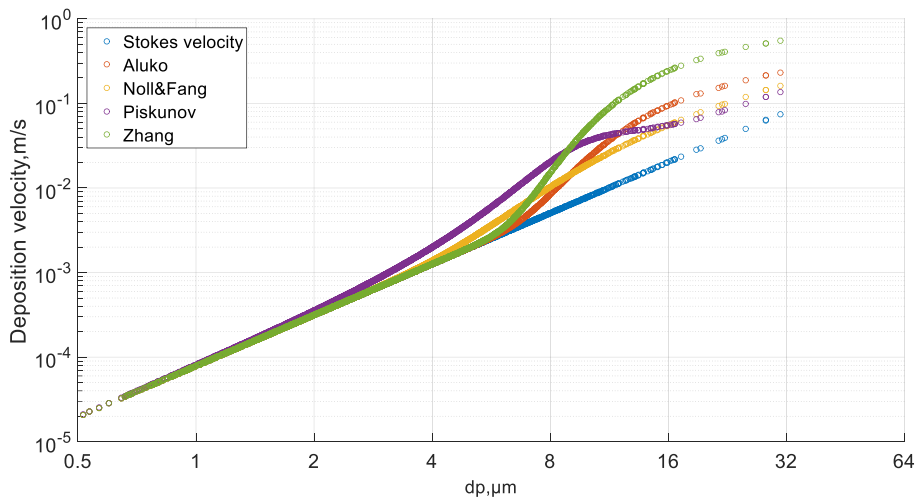
Figure 2: Deposition velocities for single particles to a smooth surface (Flat plate sampler) calculated
274 by using set of different classical deposition models for Tenerife samples (Aug 9, 2017; average wind
275 speed =3.0 m/s).

276 2.9.3 Deposition models applied to the samplers

277 **Table 1** shows the different deposition velocity models applied to the various samplers. The Piskunov
278 deposition velocity model is made for flat surfaces, and therefore it is applied to BSNE and Flat plate,
279 where deposition occurs to such surfaces. For the Sigma-2 sampler, it is assumed that each particle settles
280 with the terminal settling velocity (Tian et al., 2017), and therefore Stokes' velocity was used for
281 calculation of concentrations. In the case of MWAC, a different approach was required due to its
282 geometry. It is internally in principle an impactor design with the incoming tube pointing at the substrate,
283 but is operating at very low flow speed and therefore Reynolds numbers. As a result, it cannot be
284 described by the impactor theory only. Therefore, we assumed that the deposition velocity can't become
285 smaller than the one prescribed by the Piskunov model. As a result, we derived a velocity model based
286 on wind speed (or a reduced wind speed) and calculated the collection efficiency assuming the MWAC

to act as impactor for particles in the range of the cut-off diameter and larger. For smaller particles, we assumed that flow is like a flow over a smooth surface, so the Piskunov deposition velocity model was applied (e.g., as soon as the deposition velocity from impactor considerations becomes smaller than the Piskunov one, the latter was used).

Table 1: A summary of different deposition velocity models aplplied to the samplers

Sampler	Deposition velocity model
Sigma-2	Stokes' velocity
Flat plate	Piskunov
BSNE	Piskunov
MWAC	Combination of Piskunov and Impaction curve

2.10 Determining the size distributions for mass concentration from the free-wing impactor measurements

Considering the windows correction and the collection efficiency dependence on the impaction speed and geometry, the overall collection efficiency E is calculated according to Kandler et al. (2018). After calculating the collection efficiency, the atmospheric concentration is calculated from deposition rate and deposition velocity as

$$C = \frac{M}{V_d} = \frac{M}{E \, V_{imp}}$$ (12)

With E being the collection efficiency and v_imp the impaction velocity, calculated from ambient wind speed and rotation speed.

2.11 Determining the size distributions for mass concentration from the filter sampler measurements

Apparent number concentrations are determined from the particle deposition rate and the volumetric flow rate calculated from the mass flow for ambient conditions. The inlet efficieny (Eff_{in}) – accounting for the difference in wind speed and inlet velocity - is calculated as a function of Stokes number (Stk) (Belyaev and Levin, 1974). The ambient concentration N_{out} is calculated by dividing the measured number concentration by the inlet efficiency.

2.12 Statistical uncertainty

310 Owing to the discrete nature of the particle size measurement, the uncertainty coming from counting can

311 pose a significant contribution to the uncertainty of mass deposition rate measurement (Kandler et al.,

312 2018). It is, therefore, important to assess the uncertainties in our mass deposition rate measurements,

313 which is done in accordance to the previous work (Kandler et al., 2018). For the mass deposition rate,

314 the statistical uncertainty is assessed by a bootstrap simulation approach using Monte Carlo

315 approximation (Efron, 1979). In this work, the bootstrap simulations and the two-sided 95 % confidence

316 intervals calculation were performed by using Matlab's bootstrap function (MATLAB R2016a

317 (MathWorks, Inc). Here, MATLAB function uses a non-parametric bootstrap algorithm (Neto, 2015) to

318 compute the 95% bootstrap confidence interval.

319 # 3   Computational fluid dynamics (CFD) simulation

320 Computational fluid dynamics (CFD) simulations were conducted to predict the deposition of particles

321 on to different passive samplers (MWAC, Sigma-2 and Flat plate). A discrete phase model without

322 interaction with continuous phase was used to calculate the trajectories of the particles. The CFD software

323 ANSYS-FLUENT 18.2 was used for performing the numerical simulations.

324 **3.1   Evaluating the mean flow field**

325 In a first step the geometry of samplers was created using ANSYS DesignModeler. In a second step, an

326 enclosure around the geometry was generated. To ensure that there are no large gradients normal to the

327 boundaries at the domain boundary, the domain was created depending on the width, the height and the

328 length of the geometries. The space in front of the geometry is two times the height of the sampler, the

329 space behind the sampler is ten times the height, the space left and right of the geometry is five times the

330 width of the geometry and the space below and above the sampler is five times the height.

331 Afterwards a mesh was created using the ANSYS Meshing program. For the enhanced wall treatment

332 the first near-wall node should be placed at the dimensionless wall distance of $y^{+\wedge}\approx 1$. The dimensionless

333 wall distance is given by

334 $$y^+ = \frac{u_* y}{v} \tag{13}$$

335 With y the distance to the wall, v the kinematic viscosity of the fluid and u_* the friction velocity which

336 is defined for this purpose by

337 $$u_* = \sqrt{\tau_w / \rho} \tag{14}$$

338   With τ_w the wall, shear stress and ρ the fluid density at the wall. The wall is then subdivided into a

339   viscosity-affected region and a fully turbulent region depending on the turbulent Reynolds number Re_y

340    $$Re_y = \frac{\rho y \sqrt{k}}{\mu}$$ (**15**)

341   With y the wall-normal distance from the wall to the cell centers, k the turbulence kinetic energy and μ

342   the dynamic viscosity of the fluid. If $Re_y > 200$ the k-epsilon model is used. $Re_y < 200$ the one-equation

343   of Wolfstein is employed (Chmielewski and Gieras, 2013; Fluent, 2015). The flow field was calculated

344   by solving the Reynolds Averaged Navier Stokes's equations with the software ANSYS Fluent. Standard

345   k-epsilon model was used to calculate the Reynolds-stresses. The boundary conditions at the sides of the

346   domain were set to symmetric. The inlet boundary condition was set to 2, 4 or 8 m/s with air as fluid

347   (Density: 1.225 kg/m^3, viscosity: 1.7849*10^{-5} kg/(ms)). The outlet boundary condition was set to pressure

348   outlet.

349   The turbulence intensity $\mathbf{T_i}$ was calculated as

350    $$\mathbf{T_i} = \frac{\left(\frac{2}{3}\mathbf{k}\right)^{1/2}}{\mathbf{v}}$$ (**16**)

351   With k the turbulence intensity and v the velocity at the inlet of the domain.

352   Detail of the sampler construction and geometry are found in the electronic supplement (see **Figure S**

353   **18, S 19 and S 20**). Different cases were calculated for the Flat plate sampler (deposition area of 12 and

354   25 mm), for the Sigma-2 and for the MWAC (**Figure 3**). For the Flat plate, a mesh with 3,920,000 cells

355   was generated, for the Sigma-2 one with 7,600,000 cells and for the MWAC one with 4,620,000. After

356   the meshing, the flow fields were calculated. **Figure 3** shows as example the velocity magnitude in the

357   middle of the domain for a velocity of 4 m/s at the inlet.

358   In the last step, particles were injected into the velocity field and their trajectories computed. For all

359   samplers, the deposition area boundary condition was set to "trap" and the walls were defined as

360   reflecting boundaries. Different particle sizes (1, 2.5, 5, 10, 20 and 50 μm, Stokes' diameter) for three

361   different wind speeds (2, 4, 8 m/s) were investigated. The particles density was set to a value of 2600

362   kg/m³ to match an approximate dust bulk density. The particle concentration was $4*10^8$ /m^2 in all cases,

363   while the injection area was adjusted to the geometries (**Figure 3**).

364   The number of particles trapped in the deposition area was determined. The deposition velocity V_d was

365   calculated by

366 $$V_d = \frac{N_{pt}v}{A_d C_p}$$ (**17**)

367 with N_{pt} the number of trapped particle at the deposition area, v the velocity of the air at the inlet

368 boundary of the domain, A_d the deposition area and C_p the particle concentration at the particle injection

369 area (Sajjadi et al., 2016).

370

371
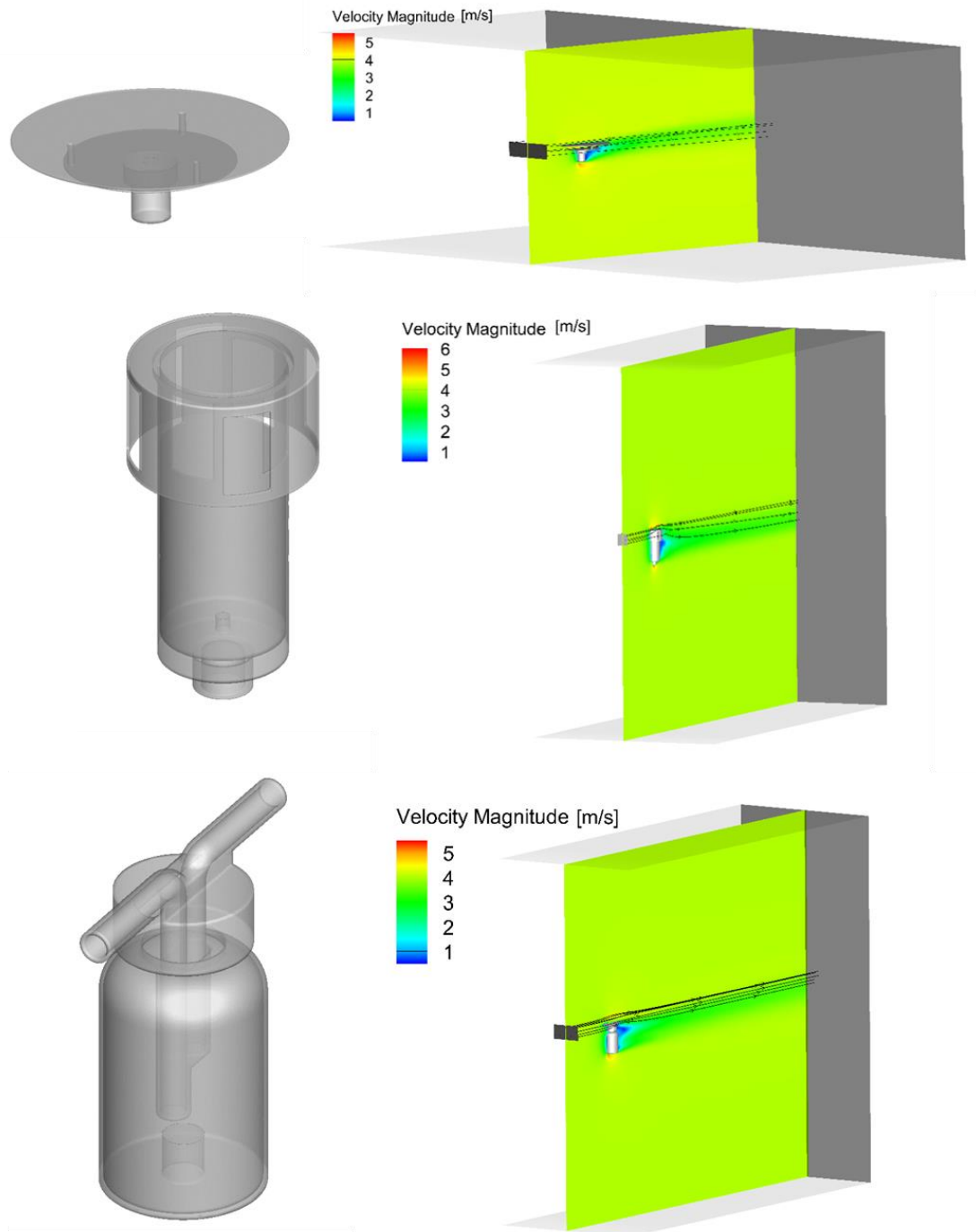
Figure 3: Geometries of Flat plate sampler (top), Sigma-2 sampler (middle), MWAC sampler (bottom). CFD modeling domain and velocity magnitude, inlet velocity: 4 m/s (right); in addition, the injection area is shown in black (Flat plate sampler: width 0.2 m, height 0.05 m; Sigma-2-sampler: width 0.2 m, height 0.1 m; Bottle sampler: width 0.1 m, height 0.05 m) along with exemplary streamtraces.

3.2 Velocity contours and vectors for the samplers

For the Flat plate sampler, stream velocities and turbulence intensities are shown in **Figure 4**. The formation of the boundary layer at the wall of the sampler is clearly visible at all velocities. At the central sampling location, the flow between the plates has the same velocity as the free stream, so for the analytical deposition models, the lower plate can be treated as single surface. The highest velocity is found at the sharp edge at the bottom of the sampler. Due to the high velocity gradients in this part there is also the highest turbulence intensity in the domain. As expected, the turbulent wake becomes smaller with increasing wind speed.
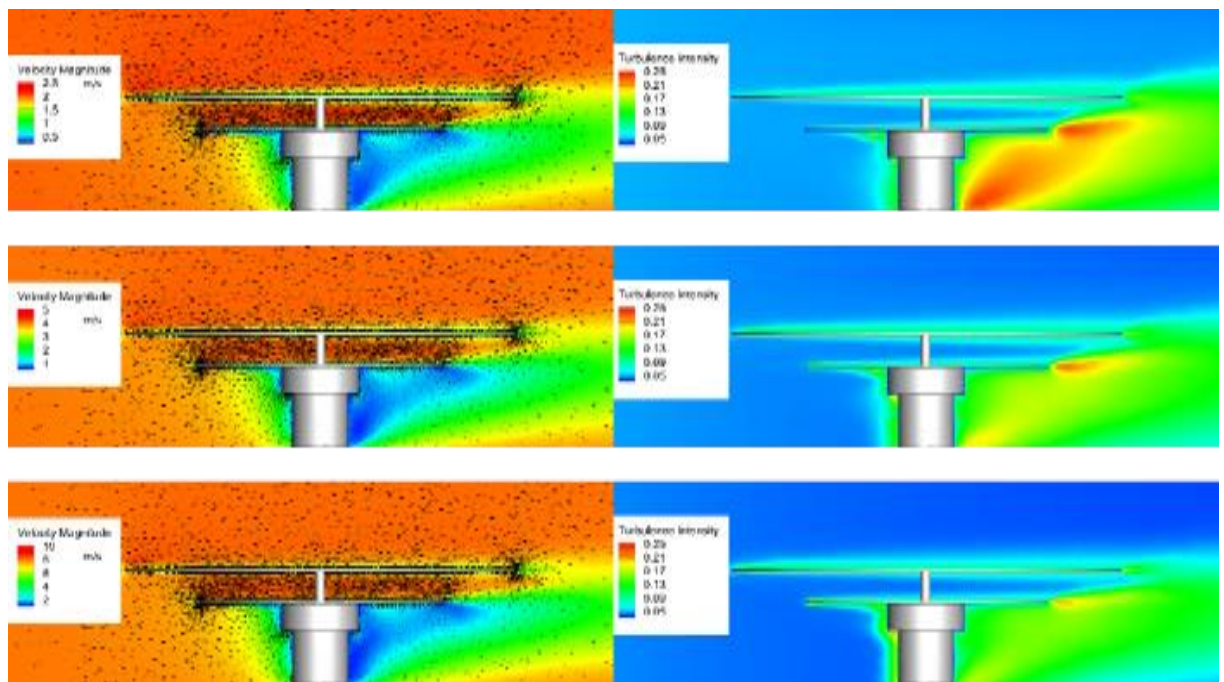
Figure 4: Flat plate Sampler: Velocity magnitude and turbulence intensity at wind speed 2 m/s (top), Flat plate Sampler: Velocity magnitude and turbulence intensity at wind speed 4 m/s (middle), Flat plate Sampler: Velocity magnitude and turbulence intensity at wind speed 8 m/s (bottom).

3.2.1 Sigma 2 Sampler

The cross section of the velocities for the Sigma-2 are shown for the 4 m/s case in **Figure S 21** in the electronic supplement. Apparently the velocity magnitude inside the sampler is much smaller than

391 outside. In the vertical settling tube, the turbulence intensity is low, justifying the idea of Stokes settling

392 inside. Owing to the open, but bulky geometry, there is a flow into the interior at the back. The highest

393 velocities and turbulence intensities are found at the sharp edges at the top and bottom of the sampler.

394 **Figure S 22** (in the electronic supplement) shows the cross section of the velocities for the MWAC in

395 the 4 m/s case. Furthermore, the velocity field and the velocity vectors in the cross sections across and

396 along the inlet tube are shown in **Figure S 23** in the electronic supplement. In the tubes the typical pipe

397 flow is formed. In the figures showing the cross sections along the inlet tube a symmetrical flow over the

398 pipe cross section is visible. Finally, **Figure S 24** (in the electronic supplement) shows the mean flow

399 velocity in the MWAC tube is shown as a function of the outside velocity for the three cases. The fitting

400 curve shows that the mean velocity in the pipe increases linearly with the external velocity.

4   Results and Discussion

401

4.1   Methodical aspects (Field Measurements)

402

403 4.1.1   Mass deposition rate comparison

404 Mineral dust was the dominating particle type during this campaign, consisting of different silicates,

405 quartz, calcite, dolomite, gypsum, similar to previous findings for this location (Kandler et al., 2007).

406 Therefore, hygroscopicity was not taken into account, as due to the mostly non-hygroscopic compounds

407 and the moderate humidities their impact was rated low. Details on the composition will be reported in a

408 companion paper.

409 The mass and number deposition rates (given per unit time and sample surface area) along with daily

410 average temperature and wind speed are presented as daily values. Details for all days and all samplers

411 can be found in the electronic supplement (see **Table S 1, S 2, S 3 and S 4**). All data shown in this section

412 are calculated from SEM measurements. Particle sizes are reported as aerodynamic diameter, if not

413 otherwise stated.

414 **Figure 5** shows as example mass deposition rates for different samplers during a dust event and a non-

415 dust event day. For all samplers, the mass deposition rate size distributions peaked in the 16-32 µm

416 diameter interval. This result is in support of the conclusion that atmospheric dry deposition is dominated

417 by coarse particles owing to their high deposition velocities (Davidson et al., 1985; Holsen et al., 1991).

418 There is a considerable difference among different samplers affecting mainly the size range with the

419 highest mass deposition rates, whereas the difference is small for smaller particles. MWAC and BSNE –

420 both horizontal flux samplers – collect coarser material than the Flat plate and Sigma-2 samplers, which

in contrary measure the vertical flux. In particular, the MWAC sampler exhibits considerably higher coarse particle mass deposition rates, probably owing to its impactor-like design.

Table 2: The campaign maximum and minimum and median mass deposition rates measured by the samplers

Samplers	Maximum deposition rate (mg/ (m^{2}d))	Minimum deposition rate (mg/ (m^{2}d))	Median deposition rate (mg/ (m^{2}d))
MWAC	1240	0.6	4.8
BSNE	310	0.2	3.1
Flat plate	80	2.0	1.1
Sigma-2	117	1.9	1.1

As consequence the vertical flux instruments collect much less material than the horizontal flux ones (**Table 2**), which is in accordance with previous findings (Goossens, 2008). In the present study, horizontal to vertical flux mass ratio is approximately between 2.8 and 4.4 (with single size intervals ranging between 2 and 50), while Goossens (2008) reported it to be in between 50 and 160. This difference in the ratio might come from the different approaches. Goossens (2008) used water as a deposition surface while in our study we used a SEM sampling substrate. Furthermore, from **Figure 5**, we can clearly see that that there is a strong variation in mass deposition rates between dust event days and non-dust event days (full dataset is shown in **Figure 6**). Generally, the temporal variation is higher than the difference between the samplers so a strict comparison between this and the previous study can't be done.
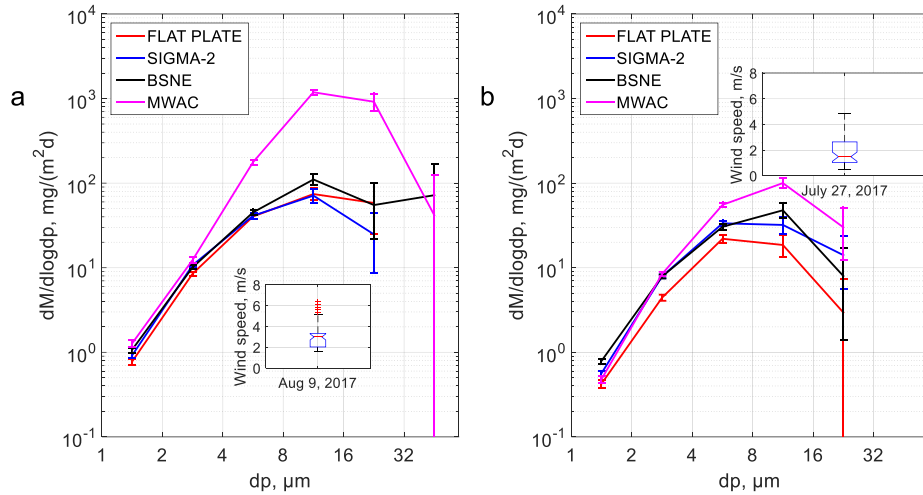
Figure 5: Size resolved mass deposition rate measured by different passive samplers: a) dust event day; b) non-dust event day. Data are derived from SEM measurements. Error bars show bootstrapped 95% confidence interval. The inserts show box plots for the wind speed distribution based on 30-min intervals.
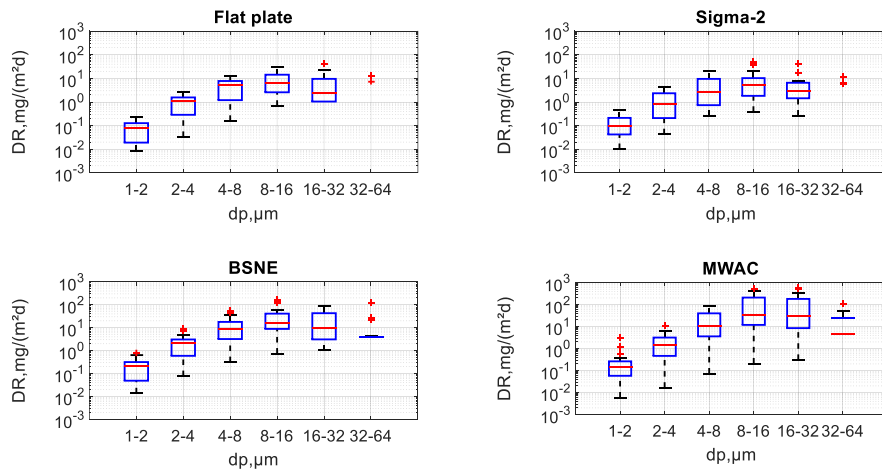
Figure 6: box-plots of size resolved deposition rate (campaign data; Flat plate, Sigma-2, MWAC and BSNE samplers). On each blue box, the central mark is the median, the edges of the box are the 25th and 75th percentiles. The red vertical lines show the standard deviation.

From the structure of the deposition models, a wind speed dependency for the deposition velocity should be expected. The average wind speed during the campaign was about 3.5 m/s with the lowest daily median around 1.5 m/s and the highest 7 m/s. A daily box-plot of 30-min averaged wind speed at Izaña is shown in **Figure S 1** in the electronic supplement.

Figure 7 shows the mass deposition rate ratio of MWAC, BSNE and Flat plate to Sigma-2 as function of wind speed. The Sigma-2 sampler was chosen for comparison, as due to its settling tube design, it is expected to have the least wind sensitivity. The results show highly scattered values. The collection efficiency of MWAC for large particles has an increasing tendency in comparison to Sigma-2 slightly with increasing wind speed, while there is barely a trend visible for the BSNE. Both – being horizontal flux samplers – collect considerably more material than the Sigma-2. For the Flat plate, the deposition velocity in relation to the Sigma-2 has a weak decreasing trend for higher wind speeds, but generally, the deposition speed is similar. Overall, the relation of Sigma-2 to BSNE shows the closest agreement, while the scatter is higher for the other combinations. More information on the relation between the other instruments is shown in **Figure S 2, S 3, S 4, S 5, S 6, S 7 and S 8** in the electronic supplement.
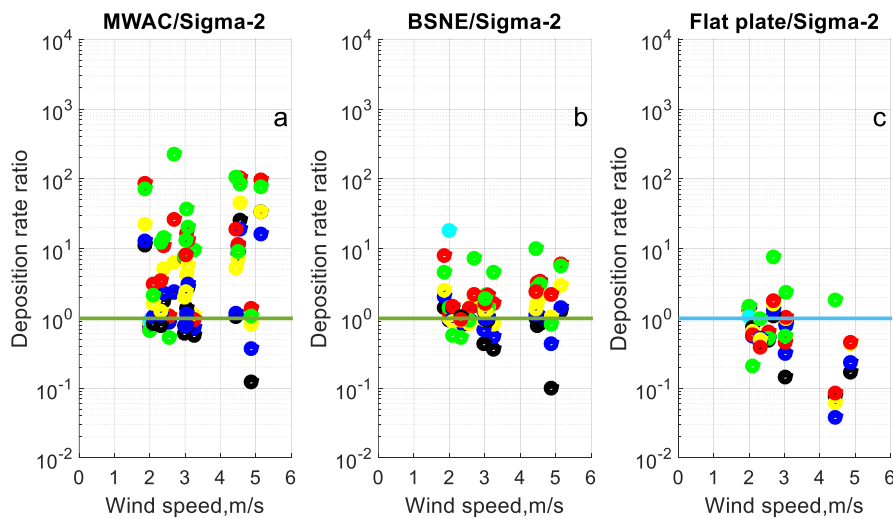

Figure 7: Deposition rate ratio as function of wind speed for different days (MWAC/ Sigma-2 (a), BSNE/Sigma-2 (b) and BSNE/ Sigma-2 (c)). Different colors represent deposition rate measured in different size intervals (black: 1-2 μm; blue: 2-4 μm; yellow: 4-8 μm; red: 8-16 μm; green: 16-32 μm; cyan: 32-64 μm).

The deposition rate ratios obtained from the measurements are identical to the deposition velocity ratios, when the sampling time and concentration are the same (eq. (7)); the latter is achieved by the close and

parallel sampling. Therefore, the experimentally determined ratios can now be compared to the deposition velocity ratios derived from the theoretical considerations. **Figure 8** shows the according comparison. Note that this consideration allows for the assessment of relative model performance and sampler efficiency, but lacking a 'true' reference, it does not allow for determining the most accurate sampler.

While for BSNE and Sigma-2 observation and model fit comparatively well, the deposition velocity is misestimated for the Flat plate/Sigma-2 pairing for all particle sizes (overestimate for Flat plate deposition velocity or/and underestimate for Sigma-2). For MWAC/Sigma-2, there is a clear size dependency, indicating that probably the impactor model overestimates the deposition velocity; the latter might be due to unaccounted particle losses (e.g., inlet efficiency). MWAC, BSNE and Sigma-2 agree with respect to deposition velocity better based on the measurement data than predicted by the theory. It may be connected to the non-stationarity of the atmosphere, which is not accounted for by the models, i.e. the permanent wind speed fluctuations smoothing out detail differences of a stationary flow. The Flat plate sampler, however, has a lower-than-predicted deposition velocity.
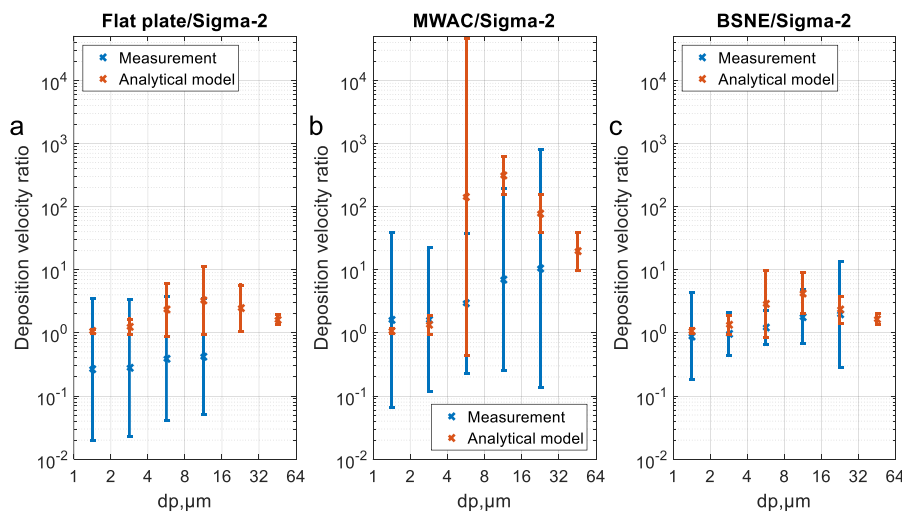
Figure 8: Comparison of geometric mean ratio of deposition velocities for different sampler pairs derived from measured deposition rates (blue) and from corresponding deposition models (orange).

(a) Flat plate/Sigma-2; (b) MWAC/Sigma-2; (c) BSNE/Sigma-2. Error bars show geometric standard deviations. According deposition models are listed in **Table 1**.

485   4.1.2   Dependence of PM_{10} dust deposition on atmospheric concentration and wind speed

486   **Figure S 16** (in the electronic supplment) and **Table 3** display for the approximate PM_{10} size range the

487   correlation between number deposition rates, atmospheric particle number concentrations measured by

488   OPC and the wind speed for different samples. For this consideration, only the overlapping size range –

489   1-10 μm aerodynamic diameter – was used. As expected, there is in all cases a positive correlation

490   between concentrations and number deposition rates (see **Figure S 16** in the electronic supplement). In

491   particular, for the BSNE and the Simga-2, robust correlations with a trend to underestimation at higher

492   concentrations exist. While the models predict a positive correlation of wind speed and deposition rate,

493   this is not observed in the measurements. Instead, a non-significant anti-correlation can be observed, if

494   at all (e.g., for Flat plate; r²: 0.319, p-value = 0.070, slope=-0.261), indicating a cross-influence of wind

495   speed and concentration. E.g. higher concentrations of dust aerosol particles might be meteorologically

496   linked to lower wind speeds due to a different transport situation. Such a general behavior was observed

497   previously for example by different techniques for a dust transport region (Kandler et al., 2011). An

498   ambiguous wind-dependency has been reported for other places (Xu et al., 2016). In this study, the main

499   driver of the deposition rate during is obviously the dust concentration.

500   **Table 3**: Summary of the regression analysis for the correlations between the dust deposition rate and

501   the atmopsheric concentrations (**PM_{10} size range; measured by the OPC**), and for the correlations

502   between the dust deposition rates and the wind speeds. Significant relationships are shown in bold.

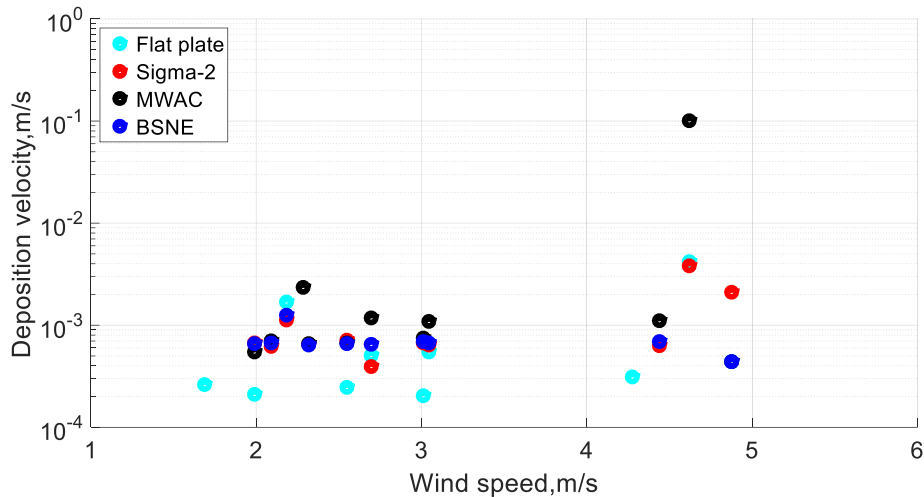|	Deposition rate vs concentration			Deposition rate vs wind speed		
	r²	p-value	slope (m/d)	r²	p-value	Slope ($1.16*10^5$ /(m^3))
Flat plate	0.600	0.0052	0.492	0.319	0.070	-0.261
MWAC	0.155	0.335	0.146	0.308	0.153	-0.157
BSNE	**0.937**	**$1.00*10^{-6}$**	**0.832**	0.017	0.706	-0.052
Sigma-2	**0.925**	**$3.39*10^{-5}$**	**0.725**	0.0125	0.775	-0.069

503

504   In a second step is was tested, whether the application of each sampler's assigned deposition model can

505   increase the correlation between the measurements by the deposition samplers and the OPC observations,

506   i.e. whether the meteorological parameters accounted for in the models can decrease the deviation.

507   Therefore, in analogy to the previous correlation, the concentrations modeled from each sampler's SEM

508 data were correlated with the OPC data for the size range between 1 and 10 μm in particle diameter (see
509 **Table S7** in the electronic supplement). However, no increase in correlation quality is observed,
510 indicating that – like already observed from the varying ratio calculations above – the deposition models
511 fail to describe the deposition behavior in detail.

512 From the correlation relations in **Table 3**, it can be learned that MWAC is least suitable for estimating
513 PM_{10}, which fully agrees well with previous studies (Mendez et al., 2016). However, the correlation
514 analysis here shows that BSNE is actually a suitable instrument for a PM_{10} estimation, which is in contrast
515 to the wind-tunnel observation of Mendez et al. (2016). This discrepancy might be owed to the different
516 approaches. While in the previous work the loss of concentration from the passing aerosol was measured,
517 in this study a gain of deposition was investigated. As result, for lower deposition velocities (discussed
518 below), the former approach will yield high uncertainties. Similar to BSNE, Flat plate and Sigma-2
519 appear good estimators for PM_{10}, which is in accordance with previous studies (Dietze et al., 2006).

4.1.2.1 Size-resolved apparent deposition velocity in the PM_{10} size range

521 **Figure 9** displays the apparent deposition velocity (calculated as the ratio of the number deposition rate
522 to the concentration of the OPC) as function of the wind speed. Obviously, also here there is not clear
523 trend. The apparent deposition velocities range between $2*10^{-4}-10^{-1}$ m/s. As can be clearly seen from the
524 plot, the effect of wind speed on deposition velocity is negligible, as indicated already in **Table 3**. While
525 this is in contradiction to the models, one has to keep in mind that the (a) the observed wind speeds are
526 comparatively low here, and (b) the considered size range is not the one most affected by the wind speed.
527 An effect of the wind speed might therefore be much stronger at higher wind speeds and for larger
528 particles.

529

Figure 9: Apparent deposition velocity: ratio of number deposition rate determined from SEM measurements to the number concentration observed by the OPC as function of wind speed. For the consideration, only the overlapping size range (approximately 1-10 µm) was used.

4.1.3 Atmospheric mass concentrations derived from deposition rates

4.1.3.1 Consistency between samplers and corresponding models

Figure 10 compares a mass deposition rate size distribution with the according concentrations derived by the modeled deposition velocities. Calculating the mass concentrations from different passive samplers with different models leads in most cases to a better agreement between the measurements, taking into account the statistical uncertainties (see **Figure S 9** in the electronic supplement). This indicates that the deposition velocity models selected for the samplers are generally suitable, despite the deviations in single cases.

541
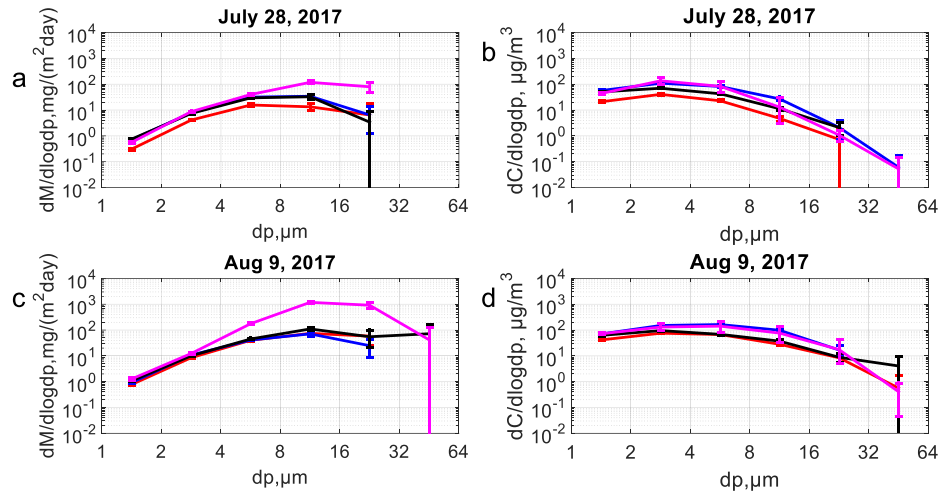
Figure 10: Comparing different samplers with respect to (a, c) dust mass deposition rates and (b, d) dust mass concentrations calculated from application of the corresponding model as function of particle size. Different colors indicate different samplers (red: Flat plate; blue: Sigma-2; black: BSNE and magenta: MWAC). Bars show the 95% confidence intervals. According deposition models for concentration calculation are given in the **Table 1**.

4.1.3.2 **Size-resolved comparison with active samplers**

The calculated number concentrations in the size interval between 1–10 μm are compared with the concentrations measured using the OPC. Similarly, the mass concentration size distributions above the PM$_{10}$ size range are validated using the FWI measurements.

Figure 11 (see also **Figure S 11 and S 12** in the electronic supplement) shows a comparison of number concentration size distributions calculated from deposition rate measurements of the Flat plate, Sigma-2, BSNE and MWAC samplers with the number size distributions measured by the OPC for different days. Overall, the number concentrations obtained from OPC measurements are slightly higher than the ones from the deposition rates, mainly for the size range 2-5 μm and for dust days. This reflects the tendency of a relative underestimation of the concentrations by the passive techniques for high concentrations, which was already visible in the correlation analysis above. In general, **Figure 11** shows that the deviation of calculated values from OPC measured values is significant.

In this context, **Figure 11** shows also the low influence of the two techniques used for u_* estimation. While the number concentrations derived using the friction velocity estimated from Wood (1981)

562 formulation are slightly higher and therefore in better agreement with the OPC data, the difference
563 appears to be negligible in general, probably owing to the relatively low wind speeds in this study.


564
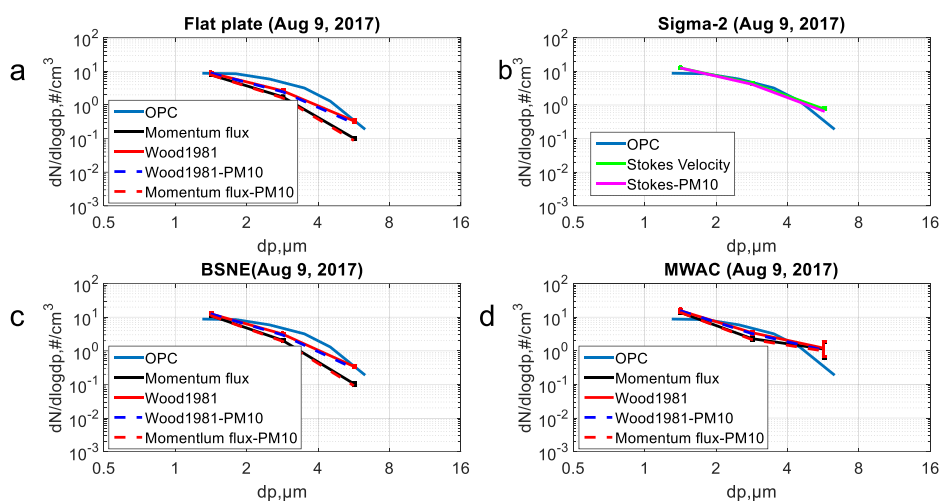
Figure 11: Comparison of the number concentrations calculated from the deposition measurements
with the number concentrations measured by the OPC. Number size distributions are obtained by
converting the SEM number deposition rates to number concentrations using the different deposition
velocity models (**Table 1**), in analogy to the mass size distributions. The blue curve shows the
concentration measurements by the OPC. For the concentrations obtained from the number deosition
rates, two different approaches for the friction velocity are shown. The black curve shows the
concentration curve calculated using the momentum flux approach without PM_{10} inlet correction (i.e.
the atmospheric concentration). The red curve shows the concentration curve calculated using the
Wood approach without PM_{10} correction. The dotted blue curve shows the concentration curve
calculated using the Wood approach with PM_{10} inlet correction (simulating the concentration the OPC
would supposedly measure). The dotted red curve shows the concentration curve calculated using the
Momentum flux approach with PM_{10} inlet correction. In case of the Sigma-2, the green curve shows the
concentrations calculated using the Stokes velocity and the magenta curve the ones using Stokes
velocity with the PM_{10} inlet correction. Bars show the central 95 % confidence interval. (a): Flat plate;
(b) Sigma-2; (c): BSNE; (d) MWAC. The average wind speed on Aug 9, 2017 was 3.0 m/s.

Figure 12 (see also **Figure S 10** in the electronic supplement) shows the comparisons for the larger
particles between the deposition-derived number concentrations and the ones from the FWI. Here, a
singnificant inconsistency occurs between the mass size distributions from passive samplers and the ones

583   from FWI. In particular, the size range larger than 10 μm seems to be generally underestimated by the

584   passive samplers. While for particles around 10 μm, this could be partly to a badly-defined collection

585   efficiency curve of the FWI ((Kandler et al., 2018); 50 % cut-off at 11 μm) and the according correction,

586   this can't be the reason for the particles larger than 16 μm, where this efficiency approaches unity. Here,

587   the deposition velocity for the samplers is apparently overestimated. A possible explanation would be

588   inlet losses of the passive sampler, but this need to be subject of further research.
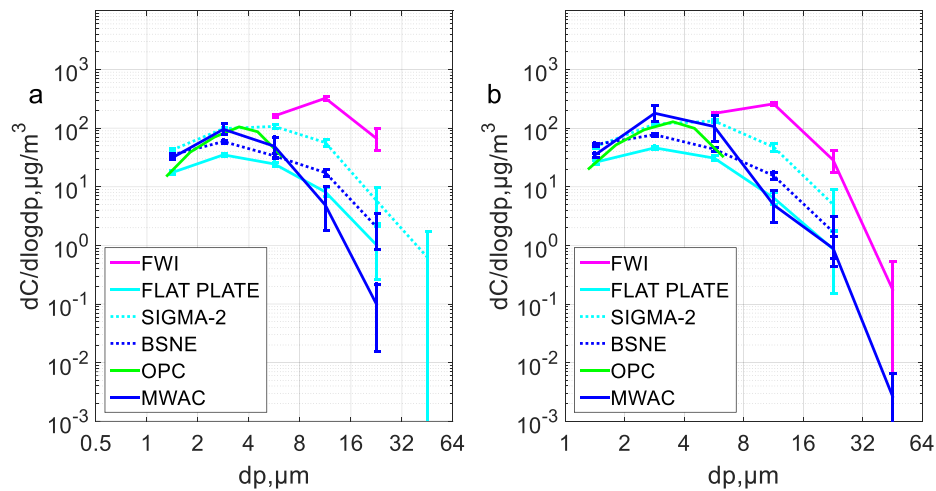
589

590   **Figure 12**: Daily average mass size distributions obtained from the passive sampler techniques in

591   comparison to an active sampler (FWI). Mass concentration size distributions were calculated from the

592   SEM mass flux measurements using the corresponding deposition velocity models. Samples were

593   collected on 26th of July (a) and 27th of July (b). The mass concentration measurements shown by the

594   FWI are daily averages (3 samples per day). Error bars show the central 95% confidence interval.

595   In a last step, the deposition-derived concentrations are compared to these determined from the iso-axial

596   filter sampler. **Figure 13** shows that, while the calculated size distributions are in good agreement with

597   the OPC ones, the filter-derived seem to relatively underestimate the concentrations. A correlation

598   analysis (R-squared: 0.681, p-value = 0.0854 and slope = 2.0394) suggests, that there is a weak positive

599   correlation between calculated number concentration from filter samples and the OPC measured

600   concentration. The same comparison to other samplers is shown in **Figure S 13, S 14 and S 15** in the

601   electronic supplement. The reasons for this weak correlation – in particular in comparison to the ones

602   from Sigma-2 and BSNE – remain unexplained by now.
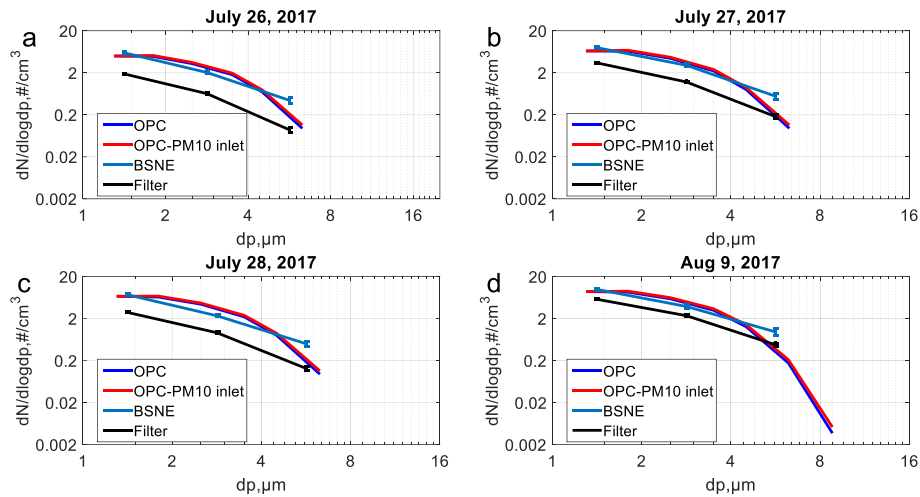
Figure 13: Number concentration size distributions obtained from the SEM analysis of the filter sampler, in comparison to BSNE and OPC for different measurement days (a: July 26, 2017; b: July 27, 2017; c: July 28, 2017; d: July 29, 2017). Number concentration size distributions from deposition are obtained by converting the SEM obtained number deposition rates to number concentration using different deposition velocity models. The red curve shows the OPC with PM_{10} inlet efficiency correction (representing the atmospheric concentration). The number concentration measurements shown for the filter sampler are daily averages. Error bars show the central 95% confidence interval.

4.1.4   Estimating the turbulent versus gravitational transport fraction

The size-resolved upward and downward deposition rates were derived from the upward-/downward facing deposition sampler by the same type of SEM analyses. Results of the size resolved-mass and number deposition rate measurements along with daily average temperatures and wind speeds are given in the electronic supplement (see **table S 5 and S 6**). The upward deposition rate is always less than the downward deposition rate. This is expected because the upward facing substrate (i.e. measuring the downward-directed deposition rate) collects particles deposited by gravitational settling and turbulent inertial impaction, while the downward facing substrate (for the upward-directed deposition rate) collects particles only by means of turbulent impaction. **Figure 14** shows the ratio of upward to downward mass deposition rate as function of particle size. The deviation is greatest for the particle size range around 8 μm, which is strongly affected by turbulence (Noll and Fang, 1989). However, nearly no trend of increasing ratio with increasing wind speed can be found here (see **Figure S 17** in the electronic supplement). Besides the wind speed magnitude, different properties were calculated from the sonic wind

624 data (e.g., turbulent intensity, Monin-Obukhov length, relative standard deviation of wind speed, average

625 vertical component), but none of them was able to explain the observed variations in the deposition rate

626 ratio.
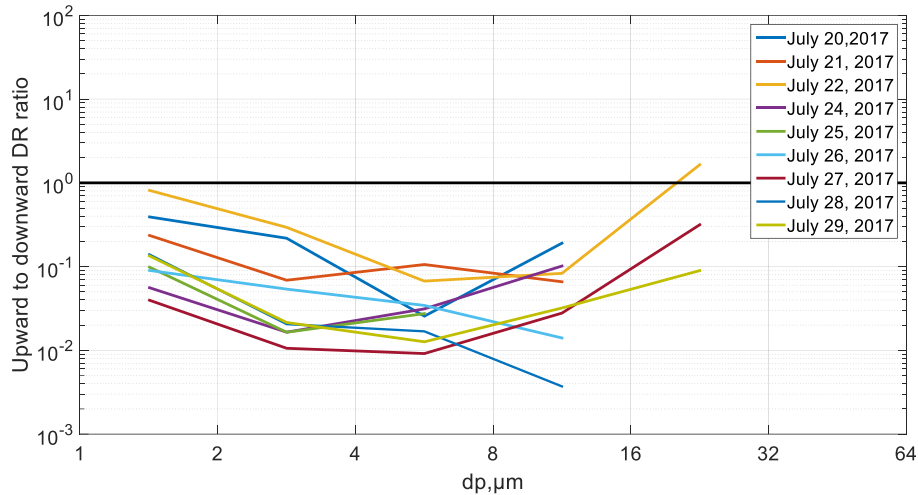
627

628 **Figure 14**: Ratio of upward- to downward-directed mass deposition rate as function of particle size.

629 The deposition rate is measured using the upward-downward-Flat plate sampler (with 25 mm stub).

4.2   Computational fluid dynamics (CFD) simulation

631 Using computational fluid dynamics (CFD), deposition velocities of particles for different passive

632 samplers were predicted and compared to the analytical deposition velocity models used for the different

633 samplers (see **Figure 15 and Figure S 25** in the electronic supplement). While for the Flat plate and

634 MWAC sampler the curves agree qualitatively (i.e. showing deposition speeds higher than Stokes

635 velocity at particles sizes 4-16 µm, which are supposedly strongest affected by turbulence), for the Sigma-

636 2, they are largely contrary except for the lowest wind velocity. The latter might be owed to the fact that

637 in a flow model, the non-omnidirectional construction of the Sigma-2 might lead to preferred airflows,

638 which are not relevant in a more variable and turbulent atmosphere. However, also for the former ones,

639 the deposition velocity curves are quantitatively largely different. **Figure S 26** (in the electronic

640 supplement) shows a comparison of the CFD-derived particle deposition velocities at different wind

641 speed values for different samplers.
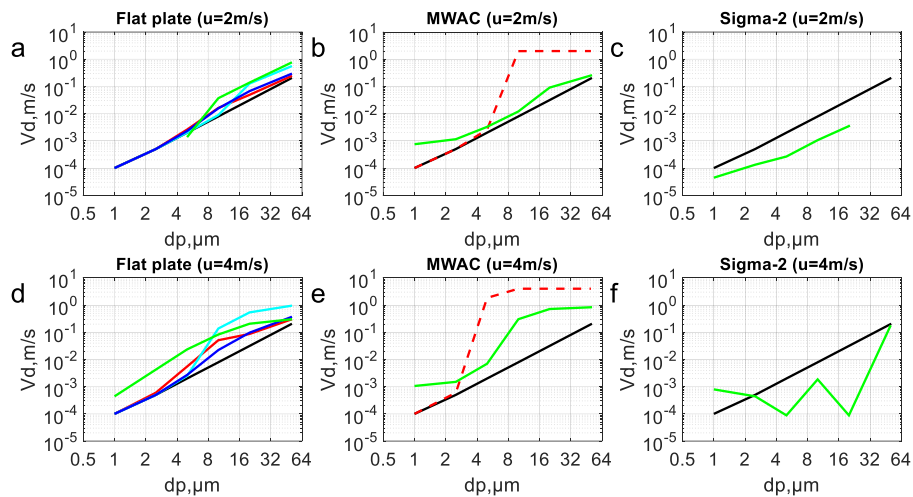
Figure 15: Deposition velocities calculated for different samplers by analytical and CFD approaches. The red curve shows the deposition velocity calculated using the Piskunov model, the dotted red curve shows the combination of the Piskunovand the impaction curve model, the black curve shows the Stokes deposition velocity, the blue curve the Noll and Fang model, the cyan the Zhang model, and the green curve finally the deposition velocity from CFD. Panels **a-c** are calculated for 2 m/s wind speed, **d-f** for 4 m/s.

4.3   Comparison of measured deposition rate ratios to analytically and CFD modeled ones

As there is no reference instrument for dry deposition sampling, the separate approaches are compared in a relative way. **Figure 16 a-c** show comparisons of the deposition velocity ratios derived from the analytical models with the according measured deposition velocity ratios (equalling the according deposition rate ratios), **d-f** the respective correlation of the ratios derived from CFD modeling with the measurement. As the CFD models could only be calculated for a limited number of flow velocities, deposition velocity values were interpolated between the calculated cases. Generally, the agreement is very poor. Practically, no variation observed in the measurement data can be explained by model variation, independently of the type of model. While this might be explained to a smaller extent by the propagating measurement uncertainties for the largest particles with low counting statistics, for the smaller ones this systematic deviation must have other reasons.
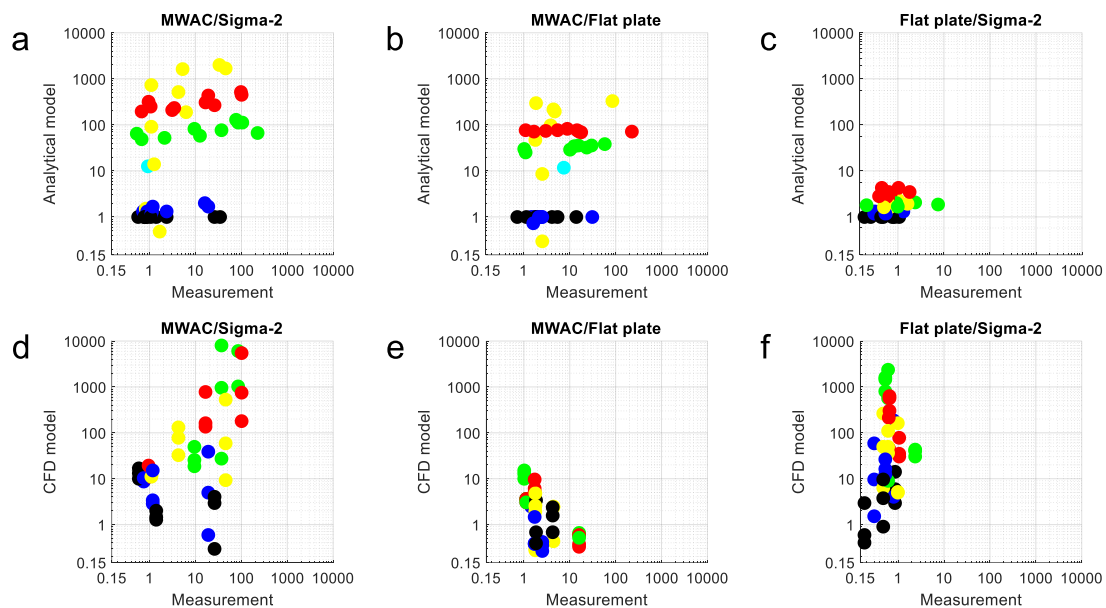
Figure 16: Comparison of the observed deposition velocity ratios with modeled ones by the analytical deposition models (upper row, a-c) and by the CFD models (lower row, d-f). (a, d) MWAC/Sigma-2; (b, e) MWAC/Flat plate; (c, f) Flat plate/Sigma-2. Multiple daily measurements are shown in each plot. Different colors represent different size intervals. 1-2 μm: Black, 2-4 μm: Blue, 4-8 μm: Yellow, 8-16 μm: Red, 16-32 μm: Green, 32-64 μm: Cyan.

5   Summary and Conclusions

Parallel dust aerosol deposition measurements by means of deposition and other passive samplers were conducted at Izaña Global Atmospheric Watch observatory continuously from 14th of July to 24th of August 2017. In addition, active aerosol collection was done with a free-wing impactor and an iso-axial filter sampler. Additional information regarding the aerosol particle size distributions has been obtained by an OPC. 316,000 single particles from 6 different samplers were analyzed by SEM-EDX, yielding size resolved deposition rates.

As known from previous studies, the total deposition rate was dominated by coarse particles (16-32 μm). A high temporal daily variability in total dust deposition rate was observed. The size resolved deposition rate measurements of different passive samplers varied significantly between the samplers under the same conditions. This was in principle expected from the different sampler construction. Applying suitable deposition velocity models, atmospheric concentrations were calculated from different sampler deposition rates. The resulting concentrations on average are in better agreement between the samplers than the deposition rates. However, discrepancies beyond the measurement uncertainty remain unexplained by the deposition models, in particular with respect to dependency on wind speed, which is

predicted by the models, but not observed. The estimation of an appropriate deposition velocity from different models for calculating atmospheric concentrations remains obviously a challenge. In particular, when considering the size-resolved deposition velocities and deposition rate ratios, great discrepancies show up. While for an integrated bulk measurement or the PM_{10} size range at least a qualitative agreement between the samplers can be reached, no model – analytical nor CFD – is able to explain the observed sampler-specific variations in deposition rate. Clearly, a better physical understanding is needed here.

In the PM_{10} size range, a good agreement is found between the calculated concentrations for samples from different passive and the concentrations measured using an OPC. For particle sizes above PM_{10}, the comparison of the deposition-derived size distributions with impactor and filter measurements shows considerable underestimates of the deposition samplers, which must be interpreted as overestimation of the large-particle deposition velocities.

Deposition velocities from different analytical deposition models are compared to ones calculated using computational fluid dynamics simulations for different samplers. The comparison shows that two methods largely disagree. Moreover, all theory-based deposition velocities (analytical as well as CFD approaches) fail to represent the observed measurement differences between the samplers. This obviously points to the need of better understanding the physics of dry deposition in general.

The correlation analysis between dust deposition rate, dust concentrations and wind speed reveals that the variation in deposition rate is mainly controlled by changes in concentration; variations in wind speed play a minor role for wind speeds lower than 6 m/s. However, the situation might be different for higher wind speeds (Kandler et al., 2018).

The correlation analysis between deposition rates and OPC measurements demonstrated that BSNE and Sigma-2 can be a good option for PM_{10} measurement, while the MWAC is not a suitable option. Apart from that result with respect to the PM_{10} size range, no recommendation for a least biased general purpose deposition sampler can be derived from our study.

Moreover, as the results show that the different samplers can't deliver consistent results between the sampler types, a recommendation must be that if a certain sampler type is chosen for a study, it should not be modified or replaced by another one for sake of consistency of results, even if it was shown that the results do not agree well for example with active sampling. The results show, nevertheless, that passive sampling techniques coupled with an automated single particle analysis provides insights into the variation of size distribution, deposition rate and concentration of atmospheric particles.

6   Acknowledgements

7   Author contribution

A. W. conducted the field measurements and did data evaluation and interpretation. K. S. helped with the field measurements, carried out the SEM analyses and did data processing. J. M. and B. E. executed the CFD model setup and calculations. S. R. operated the OPC including the data processing and the meteorological base measurements. K. K. designed the experiment, designed and prepared the sampling equipment and did data processing and interpretation. All authors contributed to the data discussion and manuscript preparation.

8   Data availability

The data sets used for this publication are available from the Pangaea repository free of charge (https://doi.pangaea.de/10.1594/PANGAEA.901413)

References

Aluko, O. and Noll, K. E.: Deposition and suspension of large, airborne particles, Aerosol Sci. Technol. , 40, 503-513, 2006.

Andreae, M. O.: Climatic effects of changing atmospheric aerosol levels, in: Future Climates of the World, World Survey of Climatology Henderson-Sellers, A. (Ed.), Elsevier, New York, 1995.

Arimoto, R.: Eolian dust and climate: relationships to sources, tropospheric chemistry, transport and deposition, Earth Sci Rev. , 54, 29-42, 2001.

Arya, S.: Suggested revisions to certain boundary layer parameterization schemes used in atmospheric circulation models, Mon Weather Rev., 105, 215-227, 1977.

Belyaev, S. and Levin, L.: Techniques for collection of representative aerosol samples, J. Aerosol Sci., 5, 325-338, 1974.

Bergamaschi, P., Bräunlich, M., Marik, T., and Brenninkmeijer, C. A.: Measurements of the carbon and hydrogen isotopes of atmospheric methane at Izaña, Tenerife: Seasonal cycles and synoptic-scale variations, J Geophys Res Atmos., 105, 14531-14546, 2000.

Chmielewski, M. and Gieras, M.: Three-zonal wall function for k-ε turbulence models, CMST, 19, 107-114, 2013.

Davidson, C. I., Lindberg, S. E., Schmidt, J. A., Cartwright, L. G., and Landis, L. R.: Dry deposition of sulfate onto surrogate surfaces, J Geophys Res Atmos., 90, 2123-2130, 1985.

Davies, C.: Particle-fluid interaction, J. Aerosol Sci 10, 477-513, 1979.

Dietze, V., Fricker, M., Goltzsche, M., and Schultz, E.: Air quality measurement in German health resorts-Part 1: Methodology and verification, Gefahrstoffe-Reinhalt. Luft. , 66, 45-53, 2006.

Dupont, S., Rajot, J. L., Labiadh, M., Bergametti, G., Alfaro, S., Bouet, C., Fernandes, R., Khalfallah, B., Lamaud, E., and Marticorena, B.: Aerodynamic Parameters Over an Eroding Bare Surface: Reconciliation of the Law of the Wall and Eddy Covariance Determinations, J. Geophys. Res. Atmos. , 123, 4490-4508, 2018.

Efron, B.: Bootstrap Methods: Another Look at the Jackknife, Ann. Statist., 7, 1-26, 1979.

764 Einstein, S. A., Yu, C.-H., Mainelis, G., Chen, L. C., Weisel, C. P., and Lioy, P. J.: Design and validation
765 of a passive deposition sampler, J. Environ. Monit., 14, 2411-2420, 2012.

766 Ettling, D.: Theoretische Meteorologie, Vieweg, Braunschweig/Wiesbaden, 1996. 1996.

767 Fluent, A.: Theory guide, Ansys Inc, 2015. 2015.

768 Fryrear, D.: A field dust sampler, J. Soil Water Conserv., 41, 117-120, 1986.

769 García, R., García, O., Cuevas, E., Cachorro, V., Barreto, A., Guirado-Fuentes, C., Kouremeti, N.,
770 Bustos, J., Romero-Campos, P., and de Frutos, A.: Aerosol optical depth retrievals at the Izaña
771 Atmospheric Observatory from 1941 to 2013 by using artificial neural networks, Atmos. Meas. Tech. ,
772 9, 53-62, 2016.

773 Giardina, M. and Buffa, P.: A new approach for modeling dry deposition velocity of particles, Atmos.
774 Environ., 180, 11-22, 2018.

775 Goossens, D.: Relationships between horizontal transport flux and vertical deposition flux during dry
776 deposition of atmospheric dust particles, J. Geophys. Res., 113, 2008.

777 Goossens, D. and Buck, B. J.: Can BSNE (Big Spring Number Eight) samplers be used to measure PM10,
778 respirable dust, PM2. 5 and PM1. 0?, Aeolian Res. , 5, 43-49, 2012.

779 Goossens, D. and Offer, Z. Y.: Wind tunnel and field calibration of six aeolian dust samplers, Atmos.
780 Environ., 34, 1043-1057, 2000.

781 Goudie, A. and Middleton, N.: Saharan dust storms: nature and consequences, Earth Sci Rev., 56, 179-
782 204, 2001.

783 Holsen, T. M., Noll, K. E., Liu, S. P., and Lee, W. J.: Dry deposition of polychlorinated biphenyls in
784 urban areas, Environ. Sci. Technol. , 25, 1075-1081, 1991.

785 Huang, K., Zhuang, G., Li, J., Wang, Q., Sun, Y., Lin, Y., and Fu, J. S.: Mixing of Asian dust with
786 pollution aerosol and the transformation of aerosol components during the dust storm over China in
787 spring 2007, J Geophys Res Atmos, 115, 2010.

788 Jaenicke, R. and Junge, C.: Studien zur oberen Grenzgröße des natürlichen Aerosols, Contrib. Atmos.
789 Phys., 40, 129-143, 1967.

790　Jickells, T., An, Z., Andersen, K. K., Baker, A., Bergametti, G., Brooks, N., Cao, J., Boyd, P., Duce, R.,
791　and Hunter, K.: Global iron connections between desert dust, ocean biogeochemistry, and climate,
792　Science, 308, 67-71, 2005.

793　Junge, C.: Air Chemistry and Radioactivity. Academic Press, New York, 1963.

794　Kandler, K., Benker, N., Bundke, U., Cuevas, E., Ebert, M., Knippertz, P., Rodríguez, S., Schütz, L., and
795　Weinbruch, S.: Chemical composition and complex refractive index of Saharan Mineral Dust at Izana,
796　Tenerife (Spain) derived by electron microscopy, Atmos. Environ. , 41, 8058-8074, 2007.

797　Kandler, K., Schneiders, K., Ebert, M., Hartmann, M., Weinbruch, S., Prass, M., and Pöhlker, C.:
798　Composition and mixing state of atmospheric aerosols determined by electron microscopy: method
799　development and application to aged Saharan dust deposition in the Caribbean boundary layer, Atmos.
800　Chem. Phys., 18, 13429-13455, 2018.

801　Kandler, K., Schütz, L., Deutscher, C., Ebert, M., Hofmann, H., Jäckel, S., Jaenicke, R., Knippertz, P.,
802　Lieke, K., and Massling, A.: Size distribution, mass concentration, chemical and mineralogical
803　composition and derived optical parameters of the boundary layer aerosol at Tinfou, Morocco, during
804　SAMUM 2006, Tellus B, 61, 32-50, 2009.

805　Kandler, K., Schütz, L., Jäckel, S., Lieke, K., Emmel, C., Müller-Ebert, D., Ebert, M., Scheuvens, D.,
806　Schladitz, A., and Šegvić, B.: Ground-based off-line aerosol measurements at Praia, Cape Verde, during
807　the Saharan Mineral Dust Experiment: microphysical properties and mineralogy, Tellus B, 63, 459-474,
808　2011.

809　Lai, A. and Nazaroff, W.: Supermicron particle deposition from turbulent chamber flow onto smooth and
810　rough vertical surfaces, Atmos. Environ. , 39, 4893-4900, 2005.

811　López-García, P., Gelado-Caballero, M. D., Santana-Castellano, D., de Tangil, M. S., Collado-Sánchez,
812　C., and Hernández-Brito, J. J.: A three-year time-series of dust deposition flux measurements in Gran
813　Canaria, Spain: A comparison of wet and dry surface deposition samplers, Atmos. Environ., 79, 689-694,
814　2013.

815　Mendez, M. J., Funk, R., and Buschiazzo, D. E.: Efficiency of Big Spring Number Eight (BSNE) and
816　Modified Wilson and Cook (MWAC) samplers to collect PM10, PM2. 5 and PM1, Aeolian Res., 21, 37-
817　44, 2016.

818   Neto, E. C.: Speeding up non-parametric bootstrap computations for statistics based on sample moments
819   in small/moderate sample size applications, PLoS One, 10, e0131333, 2015.

820   Nicolas, M., Ndour, M., Ka, O., D'Anna, B., and George, C.: Photochemistry of atmospheric dust: ozone
821   decomposition on illuminated titanium dioxide, Environ. Sci. Technol., 43, 7437-7442, 2009.

822   Noll, K. E. and Fang, K. Y.: Development of a dry deposition model for atmospheric coarse particles,
823   Atmos. Environ., 23, 585-594, 1989.

824   Noll, K. E., Jackson, M. M., and Oskouie, A. K.: Development of an atmospheric particle dry deposition
825   model, Aerosol Sci. Technol. , 35, 627-636, 2001.

826   Ott, D. K., Cyrs, W., and Peters, T. M.: Passive measurement of coarse particulate matter, PM10–2.5, J.
827   Aerosol Sci 39, 156-167, 2008.

828   Ott, D. K. and Peters, T. M.: A shelter to protect a passive sampler for coarse particulate matter, PM10−
829   2.5, Aerosol Sci. Technol., 42, 299-309, 2008.

830   Penner, J. E., Andreae, M., Annegarn, H., Barrie, L., Feichter, J., Hegg, D., Jayaraman, A., Leaitch, R.,
831   Murphy, D., and Nganga, J.: Aerosols, their direct and indirect effects. In: Climate Change 2001: The
832   Scientific Basis. Contribution of Working Group I to the Third Assessment Report of the
833   Intergovernmental Panel on Climate Change, Cambridge University Press, 2001.

834   Piskunov, V.: Parameterization of aerosol dry deposition velocities onto smooth and rough surfaces, J.
835   Aerosol Sci, 40, 664-679, 2009.

836   Prospero, J. M., Schmitt, R., Cuevas, E., Savoie, D., Graustein, W., Turekian, K., Volz-Thomas, A., Diaz,
837   A., Oltmans, S., and Levy, H.: Temporal variability of summer-time ozone and aerosols in the free
838   troposphere over the eastern North Atlantic, Geophys. Res. Lett., 22, 2925-2928, 1995.

839   Rodríguez, S., Cuevas, E., Prospero, J., Alastuey, A., Querol, X., López-Solano, J., García, M., and
840   Alonso-Pérez, S.: Modulation of Saharan dust export by the North African dipole, Atmos. Chem. Phys.,
841   15, 7471-7486, 2015.

842   Sajjadi, H., Tavakoli, B., Ahmadi, G., Dhaniyala, S., Harner, T., and Holsen, T.: Computational fluid
843   dynamics (CFD) simulation of a newly designed passive particle sampler, Environ. Pollut. , 214, 410-
844   418, 2016.

845   Schlichting, H.: Boundary-layer theory, McGraw-Hill, 1968.

846 Schultz, E.: Größendifferenzierende Messung der Partikeldepositionsrate, Gefahrstoffe-Reinhalt. Luft. ,

847 49, 113-118, 1989.

848 Schulz, M., Prospero, J. M., Baker, A. R., Dentener, F., Ickes, L., Liss, P. S., Mahowald, N. M., Nickovic,

849 S., Garcia-Pando, C. P., and Rodríguez, S.: Atmospheric transport and deposition of mineral dust to the

850 ocean: implications for research needs, Environ. Sci. Technol. , 46, 10390-10404, 2012.

851 Shao, Y., Ishizuka, M., Mikami, M., and Leys, J.: Parameterization of size-resolved dust emission and

852 validation with measurements, J Geophys Res Atmos, 116, 2011.

853 Slinn, S. and Slinn, W.: Predictions for particle deposition on natural waters, Atmos. Environ., 14, 1013-

854 1016, 1980.

855 Tian, Z., Dietze, V., Sommer, F., Baum, A., Kaminski, U., Sauer, J., Maschowski, C., Stille, P., Cen, K.,

856 and Gieré, R.: Coarse-particle passive-sampler measurements and single-particle analysis by transmitted

857 light microscopy at highly frequented motorways, Aerosol Air Qual Res., 17, 1939, 2017.

858 VDI2119: Ambient air measurements sampling of atmospheric particles > 2.5μm on an acceptor surface

859 using the Sigma-2 passive sampler. Characterization by optical microscopy and calculation of number

860 settling rate and mass concentration. In: Verlag des Vereins Deutscher Ingenieure, Berlin, ICS:

861 13.040.01, Beuth Verlag, Berlin, 2013.

862 Wagner, J. and Leith, D.: Passive aerosol sampler. Part I: Principle of operation, Aerosol Sci. Technol. ,

863 34, 186-192, 2001a.

864 Wagner, J. and Leith, D.: Passive aerosol sampler. Part II: Wind tunnel experiments, Aerosol Sci.

865 Technol. , 34, 193-201, 2001b.

866 Wilson, S. J. and Cook, R. U.: Wind erosion. In: Soil Erosion M.J. Kirkby, a. R. P. C. M. (Ed.), 631.45

867 S6, John Wiley & Sons, Chichester, 1980.

868 WMO: GAW Report, 202. Workshop on Modelling and Observing the Impacts of Dust

869 Transport/Deposition on Marine Productivity (7-9 March 2011), Sliema, Malta, 2011.

870 Wood, N.: A simple method for the calculation of turbulent deposition to smooth and rough surfaces, J.

871 Aerosol Sci., 12, 275-290, 1981.

872   Xu, L., Mu, G., He, J., Yang, F., Ren, X., Wan, D., and Lin, Y.: Variability of dust mass concentrations

873   and deposition rates under different weather conditions in Cele Oasis, southern Tarim Basin, Environ.

874   Earth Sci., 75, 639, 2016.

875   Yamamoto, N., Hikono, M., Koyama, H., Kumagai, K., Fujii, M., and Yanagisawa, Y.: A passive sampler

876   for airborne coarse particles, J. Aerosol Sci, 37, 1442-1454, 2006.

877